Construction of Customized Mass-Stiffness Pairs Using Templates

Carlos A. Felippa[1]

Abstract: This paper is a tutorial exposition of the template approach to the construction of customized mass-stiffness pairs for selected applications in structural dynamics. The exposition focuses on adjusting the mass matrix while a separately provided stiffness matrix is kept fixed. Two well known kinetic-energy discretization methods described in finite-element method (FEM) textbooks since the mid-1960s lead to diagonally lumped and consistent mass matrices, respectively. These two models are sufficient to cover many engineering applications. Occasionally, however, they fall short. The gap can be filled with a more general approach that relies on the use of templates. These are algebraic forms that carry free parameters. This approach is discussed in this paper using one-dimensional structural elements as examples. Templates have the virtue of producing a set of mass matrices that satisfy certain a priori constraint conditions such as symmetry, nonnegativity, invariance, and momentum conservation. In particular, the diagonally lumped and consistent versions can be obtained as instances. Thus those standard models are not excluded. Availability of free parameters, however, allows the mass matrix to be customized to special needs, such as high precision vibration frequencies or minimally dispersive wave propagation. An attractive feature of templates for FEM programming is that only one element implementation as module with free parameters is needed, and need not be recoded when the application problem class changes.

DOI: 10.1061/(ASCE)0893-1321(2006)19:4(241)

CE Database subject headings: Finite elements; Structural dynamics; Mass; Vibration; Bending; Beams; Stiffness.

Introduction

Two standard procedures for building finite-element mass matrices have been known and widely used since the mid-1960s, leading to consistent and diagonally lumped forms. These models are denoted by $\mathbf{M}_C$ and $\mathbf{M}_L$, respectively, in the sequel. Abbreviations CMM and DLMM, respectively, will be also used. Collectively these take care of many engineering applications in structural dynamics. Occasionally, however, they fall short. The gap can be filled with a more general approach that relies on *templates*. These are algebraic forms that carry free parameters. This approach is covered in this paper using one-dimensional structural elements as expository examples.

The template approach has the virtue of generating a set of mass matrices that satisfy certain a priori constraints such as symmetry, nonnegativity, invariance, and momentum conservation. In particular, the diagonally lumped and consistent mass matrices can be obtained as instances. Thus those standard models are not excluded. Availability of free parameters, however, allows the mass matrix to be *customized* to special needs such as high precision in vibration analysis, or minimally dispersive wave propagation. This versatility will be evident from the examples. The set of parameters is called the *template signature*, and uniquely characterizes an element instance.

An attractive feature of templates for finite-element methods (FEM) programming is that each "custom mass matrix" need not be coded and tested individually. It is sufficient to implement the template as a single element-level module, with free parameters as arguments, and simply adjust the signature to the problem at hand. In particular the same module should be able to produce the conventional CMM and DLMM models, which can provide valuable crosschecking.

Customization Scenarios

The ability to customize the mass matrix is not free of cost. The derivation is more complicated, even for one-dimensional (1D) elements, than those based on standard procedures. In fact, hand computations rapidly become unfeasible. Help from a computer algebra system (CAS) is needed to complete the task. When is this additional work justified? Two scenarios can be mentioned.

The first is *high fidelity systems*. Dynamic analysis covers a wide range of applications. There is a subclass that calls for a level of simulation precision beyond that customary in engineering analysis. Examples are deployment of precision structures, resonance analysis of machinery or equipment, adaptive active control, ultrasonics imaging, signature detection, radiation loss in layered circuits, and molecular- and crystal-level simulations in micro- and nanomechanics.

In structural static analysis an error of 20 or 30% in peak stresses is not cause for alarm—such discrepancies are usually covered adequately by safety factors. But a similar error in frequency analysis or impedance response of a high fidelity system may be disastrous. Achieving acceptable precision with a fine

[1]Dept. of Aerospace Engineering Sciences and Center for Aerospace Structures, Campus Box 429, Univ. of Colorado, Boulder, CO 80309-0429. E-mail: carlos.felippa@colorado.edu

Note. Discussion open until March 1, 2007. Separate discussions must be submitted for individual papers. To extend the closing date by one month, a written request must be filed with the ASCE Managing Editor. The manuscript for this paper was submitted for review and possible publication on October 20, 2005; approved on January 6, 2006. This paper is part of the ***Journal of Aerospace Engineering***, Vol. 19, No. 4, October 1, 2006. ©ASCE, ISSN 0893-1321/2006/4-241–258/$25.00.

mesh, however, can be expensive. Model adaptivity comes to the rescue in statics; but this is less effective in dynamics on account of the time dimension. Customized elements may provide a practical solution: achieving adequate accuracy with a coarse regular mesh.

A second possibility is that the stiffness matrix comes from a method that *avoids displacement shape functions*. For example, assumed-stress or assumed strain elements. (Or, it could simply be an array of numbers provided by a black-box program, with no documentation explaining its source.) Under this scenario the concept of "consistent mass matrix," in which velocity shape functions are taken to coincide with displacement ones, loses its comfortable variational meaning. One way out is to take the mass matrix of an element with similar geometry and freedom configuration derived with shape functions, and to pair it with the given stiffness. But in certain cases, notably when the FEM model has rotational freedoms, this may not be easy or desirable.

Parametrization Techniques

There are several ways to parametrize mass matrices. Three techniques found effective in practice are summarized in the following. All of them are illustrated in the worked out examples of the sections entitled "Two-Node Bar Element," "Three-Node Bar Element," and "Two-Node Timoshenko Beam Element."

Matrix-Weighted Parametrization

A matrix-weighted mass template for element e is a linear combination of $(k+1)$ component mass matrices, $k \geqslant 1$ of which are weighted by parameters

$$\mathbf{M}^e \overset{\text{def}}{=} \mathbf{M}_0^e + \mu_1 \mathbf{M}_1^e + \cdots + \mu_k \mathbf{M}_k^e \tag{1}$$

Here $\mathbf{M}_0^e$ is the *baseline mass matrix*. This should be an acceptable mass matrix on its own if $\mu_1 = \cdots = \mu_k = 0$. The simplest instance of Eq. (1) is a linear combination of the consistent and diagonally lumped masses

$$\mathbf{M}^e \overset{\text{def}}{=} (1-\mu)\mathbf{M}_C^e + \mu \mathbf{M}_L^e \tag{2}$$

This can be reformatted as Eq. (1) by writing $\mathbf{M}^e = \mathbf{M}_C^e + \mu(\mathbf{M}_L^e - \mathbf{M}_C^e)$. Here $k=1$, the baseline is $\mathbf{M}_0^e \equiv \mathbf{M}_C^e$, $\mu \equiv \mu_1$ and $\mathbf{M}_1^e$ is the "consistent mass deviator" $\mathbf{M}_L^e - \mathbf{M}_C^e$. Expression (2) is often abbreviated as "LC-weighted mass matrix."

A matrix-weighted mass template represents a tradeoff. It cuts down on the number of free parameters. Such a reduction is essential for two-dimensional (2D) and three-dimensional elements. It makes it easier to satisfy conservation and nonnegativity conditions through appropriate choice of the $\mathbf{M}_i^e$. On the minus side it generally spans only a subspace of acceptable matrices.

Spectral Parametrization

This has the form

$$\mathbf{M}^e \overset{\text{def}}{=} \mathbf{H}^T \mathbf{D}_\mu \mathbf{H}, \quad \mathbf{D}_\mu = \mathbf{diag}[c_0\mu_0 \quad c_1\mu_1 \cdots c_k\mu_k] \tag{3}$$

in which $\mathbf{H}$=generally full matrix. Parameters $\mu_0 \cdots \mu_k$ appear as entries of the diagonal matrix $\mathbf{D}_\mu$. Scaling coefficients c_i may be introduced for convenience. Some of the μ coefficients may be preset from a priori conservation conditions.

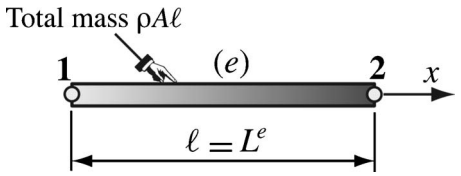

Fig. 1. Two-node prismatic bar element

Configuration (3) occurs naturally when the mass matrix is constructed first in generalized coordinates, followed by transformation to physical coordinates via $\mathbf{H}$. If the generalized mass is derived using mass-orthogonal functions (e.g., Legendre polynomials in 1D elements), the unparametrized generalized mass $\mathbf{D}=\mathbf{diag}[c_0 \quad c_1 \cdots c_k]$ is diagonal. Parametrization is effected by scaling entries of this matrix. Some entries may be left fixed, however, to satisfy a priori constraints.

Expanding Eq. (3) and collecting matrices that multiply μ_i leads to a matrix weighted combination form (1) in which each $\mathbf{M}_i^e$ is a rank-one matrix. The analogy with the spectral representation theorem of symmetric matrices is obvious. But in practice it is usually better to work directly with the congruential representation (3).

Entry-Weighted Parametrization

An entry-weighted mass template applies parameters directly to every entry of the mass matrix, except for a priori constraints on symmetry, invariance and conservation. This form is the most general one and can be expected to lead to best possible solutions. But it is restricted to simple (usually 1D) elements because the number of parameters grows quadratically in the matrix size, whereas for the other two schemes it grows linearly.

Combined Approach

A hierarchical combination of parametrization schemes can be used to advantage if the kinetic energy can be naturally decomposed from physics. For example the Timoshenko beam element covered in the section entitled "Two-Node Timoshenko Beam Element" uses a two-matrix-weighted template form similar to Eq. (2) as top level. The two components are constructed by spectral and entry-weighted parametrization, respectively.

Two-Node Bar Element

The template concept is best grasped through an example that involves the simplest structural finite element: the two-node prismatic bar of density ρ, area A and length ℓ, moving along x. See Fig. 1. The most general form of the 2×2 mass matrix form is the entry-weighted template

$$\mathbf{M}^e = \begin{bmatrix} M_{11}^e & M_{12}^e \\ M_{21}^e & M_{22}^e \end{bmatrix} = M^e \begin{bmatrix} \mu_{11} & \mu_{12} \\ \mu_{21} & \mu_{22} \end{bmatrix} = \rho A\, \ell \begin{bmatrix} \mu_{11} & \mu_{12} \\ \mu_{21} & \mu_{22} \end{bmatrix} \tag{4}$$

The first form is merely a list of entries. To parametrize it, the total element mass $M^e = \rho A \ell$ is taken out as a factor. The free parameters μ_{11} through μ_{22} are simply numbers. This illustrates a basic convenience rule: *Free template parameters should be dimensionless*. To cut down on the number of free parameters one looks at *mass property constraints*. The most common ones are

J. Aerosp. Eng., 2006, 19(4): 241-258

- Matrix symmetry: $\mathbf{M}^e=(\mathbf{M}^e)^T$. For Eq. (4) this requires $\mu_{21}=\mu_{12}$.
- Physical symmetry: For a prismatic bar $\mathbf{M}^e$ must exhibit antidiagonal symmetry: $\mu_{22}=\mu_{11}$.
- Conservation of total translational mass: Same as conservation of linear momentum or of kinetic energy. Apply the uniform velocity field $\dot{u}=v$ to the bar. The associated nodal velocity vector is $\dot{\mathbf{u}}^e=\mathbf{v}^e=v[1\quad 1]^T$. The kinetic energy is $T^e=(1/2)(\mathbf{v}^e)^T\mathbf{M}^e\mathbf{v}^e=(1/2)M^ev^2(\mu_{11}+\mu_{12}+\mu_{21}+\mu_{22})$. This must equal $(1/2)M^ev^2$, whence $\mu_{11}+\mu_{12}+\mu_{21}+\mu_{22}=1$.
- Nonnegativity: $\mathbf{M}^e$ should not be indefinite. (This is not an absolute must, and it is actually relaxed in the Timoshenko beam element discussed in the section entitled "Two-Node Timoshenko Beam Element".) Whether checked by computing eigenvalues or principal minors, this constraint is nonlinear and of inequality type. Consequently it is not often applied ab initio, unless the element is quite simple, as in this case.

On applying the symmetry and conservation rules three parameters of Eq. (4) are eliminated. The remaining one, called μ, is taken for convenience to be $\mu_{11}=\mu_{22}=(1/6)(2+\mu)$ and $\mu_{12}=\mu_{21}=(1/6)(1-\mu)$, which gives

$$\mathbf{M}^e_\mu=\frac{1}{6}\rho A\,\ell\begin{bmatrix}2+\mu & 1-\mu\\ 1-\mu & 2+\mu\end{bmatrix}=(1-\mu)\frac{1}{6}\rho A\,\ell\begin{bmatrix}2 & 1\\ 1 & 2\end{bmatrix}+\mu\frac{1}{2}\rho A\,\ell\begin{bmatrix}1 & 0\\ 0 & 1\end{bmatrix}=(1-\mu)\mathbf{M}^e_C+\mu\mathbf{M}^e_L \tag{5}$$

Expression (5) shows that the one-parameter template can be presented as a linear combination of the well known consistent and diagonally-lumped mass matrices. So starting with the general entry-weighted form (4) we end up with a two-matrix-weighted form befitting Eq. (2). If $\mu=0$ and $\mu=1$, Eq. (5) reduces to $\mathbf{M}^e_C$ and $\mathbf{M}^e_L$, respectively. This illustrates another desirable property: The CMM and DLMM models ought to be instances of the template.

Finally we can apply the nonnegativity constraint. For the two principal minors of $\mathbf{M}^e_\mu$ to be nonnegative, $2+\mu\geqslant 0$ and $(2+\mu)^2-(1-\mu)^2=3+6\mu\geqslant 0$. Both are satisfied if $\mu\geqslant -(1/2)$. Unlike the others, this constraint is of inequality type, and only limits the range of μ.

The remaining task is to find μ. This is done by introducing an *optimality criterion that fits the problem at hand*. This is where customization comes in. Even for this simple case the answer is not unique. Thus the sentence "the best mass matrix for the two-node bar is so-and-so" has no unique meaning. Two specific optimization criteria are studied in the following.

Best μ by Angular Momentum Preservation

Allow the bar to move in the $\{x,y\}$ plane by expanding its nodal degrees of freedom (DOF) to $\mathbf{u}^e=[u_{x1}\quad u_{y1}\quad u_{x2}\quad u_{y2}]^T$ so Eq. (5) becomes a 4×4 matrix

$$\mathbf{M}^e_\mu=\frac{1}{6}\rho A\,\ell\begin{bmatrix}2+\mu & 0 & 1-\mu & 0\\ 0 & 2+\mu & 0 & 1-\mu\\ 1-\mu & 0 & 2+\mu & 0\\ 0 & 1-\mu & 0 & 2+\mu\end{bmatrix} \tag{6}$$

Apply a uniform angular velocity $\dot{\theta}$ about the midpoint. The associated node velocity vector at $\theta=0$ is $\dot{\mathbf{u}}^e=(1/2)\,\ell\dot{\theta}[0\quad -1\quad 1\quad 0]^T$. The discrete and continuum energies are

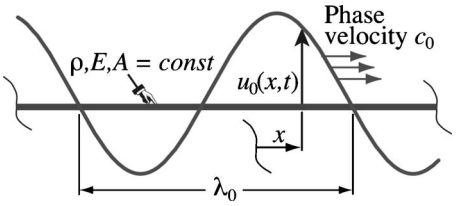

Fig. 2. Propagation of a harmonic wave over an infinite, continuum prismatic bar. The wave-profile axial displacement $u(x,t)$ is plotted normal to the bar.

$$T^e_\mu=\frac{1}{2}(\dot{\mathbf{u}}^e)^T\mathbf{M}^e_\mu\dot{\mathbf{u}}^e=\frac{1}{24}\rho A\ell^3(1+2\mu)$$

$$T^e=\int_{-\ell/2}^{\ell/2}\rho A(\dot{\theta}x)^2dx=\frac{1}{24}\rho A\ell^3 \tag{7}$$

Matching $T^e_\mu=T^e$ gives $\mu=0$. So according to this criterion the optimal mass matrix is the consistent one (CMM). Note that if $\mu=1$, $T^e_\mu=3T^e$, whence the DLMM overestimates the rotational (rotary) inertia by a factor of 3.

Best μ by Fourier Analysis

Another useful optimization criterion is the fidelity with which planes waves are propagated over a bar element lattice, when compared to the case of a continuum bar pictured in Fig. 2.

Symbols used for propagation of harmonic waves are collected in Table 1 for the reader's convenience. (Several of these are reused in the sections entitled "Two-Node Bar Element" and "Three-Node Bar Element.") The discrete counterpart of Fig. 2 is shown in Fig. 3. This is a lattice of repeating two-node bar elements of length ℓ. Lattice wave propagation nomenclature is similar to that defined for the continuum case in Table 1, but without zero subscripts.

Table 1. Nomenclature for Harmonic Wave Propagation in a Continuum Bar

Quantity	Meaning (physical dimensions in brackets)
ρ, E, A	Mass density, elastic modulus, and cross section area of bar, respectively
$\rho\ddot{u}_0=Eu_0''$	Bar wave equation; alternate forms: $-\omega_0^2u=c_0^2u''$ and $u''+k_0^2u=0$
$u_0(x,t)$	Waveform $u_0=B_0\exp(i(k_0x-\omega_0t))$ [L], in which $i=\sqrt{-1}$
B_0	Wave amplitude [L]
λ_0	Wavelength [L]
k_0	Wave number $k_0=2\pi/\lambda_0$ [1/L]
ω_0	Circular (also known as angular) frequency $\omega_0=k_0c_0=2\pi f_0=2\pi c_0/\lambda_0$ [rad/T]
f_0	Cyclic frequency $f_0=\omega_0/(2\pi)$[cycles/T (Hz/s)]
T_0	Period $T_0=1/f_0=2\pi/\omega_0=\lambda_0/c_0$ [T]
c_0	Phase velocity $c_0=\omega_0/k_0=\lambda_0/T_0=\lambda_0f_0=\sqrt{E/\rho}$ [L/T]
κ_0	Dimensionless wave number $\kappa_0=k_0\lambda_0$ ($\kappa_0=2\pi$ in continuum)
Ω_0	Dimensionless circular frequency $\Omega_0=\omega_0T_0=\omega_0\lambda_0/c_0$

Note: Zero subscripted quantities, such as k_0 or c_0, refer to the continuum bar. Unsubscripted counterparts, such as k or c, pertain to a discrete FEM lattice as in Fig. 3.

J. Aerosp. Eng., 2006, 19(4): 241-258

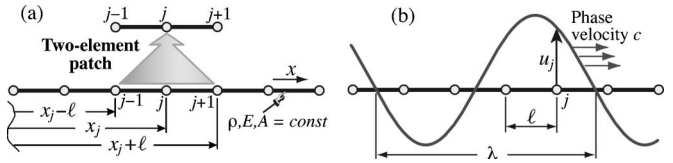

Fig. 3. An infinite lattice of two-node prismatic bar elements: (a) Two-element patch extracted from lattice; (b) characteristic dimensions for a propagating harmonic wave

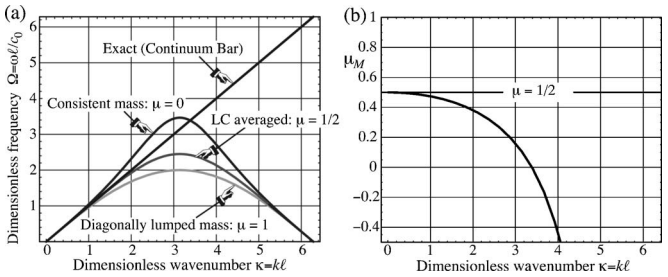

Fig. 4. Results from Fourier analysis of two-node bar lattice: (a) Dispersion curves for various choices of μ; (b) wave number dependent μ_M that makes lattice match the continuum

The lattice propagation process is governed by the semidiscrete equation of motion $\mathbf{M\ddot{u}+Ku=0}$, which can be solved by Fourier methods. To study solutions it is sufficient to extract a two-element patch as illustrated in Fig. 3(a). Within some constraints noted later the lattice can propagate travelling harmonic waves of wavelength λ and phase velocity c, as depicted in Fig. 3(b). The wave number is $k=2\pi/\lambda$ and the circular frequency $\omega=2\pi/T=2\pi c/\lambda=kc$. Fig. 3(b) displays two characteristic lengths: λ and ℓ. The element-to-wavelength ratio is called $\chi=\ell/\lambda$. This ratio characterizes the fineness of the discretization with respect to wavelength. A harmonic wave of amplitude B is described by the function

$$u(x,t)=B\exp[i(kx-\omega t)]=B\exp[i(\kappa x-\Omega c_0 t)/\ell\,],\quad i=\sqrt{-1} \tag{8}$$

Here the dimensionless wave number κ and circular frequency Ω are defined as $\kappa=k\ell=2\pi\ell/\lambda=2\pi\chi$ and $\Omega=\omega\ell/c_0$, respectively, in which $c_0=\sqrt{E/\rho}$ is the continuum bar wave speed.

Using the well-known bar stiffness matrix and the mass template (5) gives the patch equations

$$\frac{\rho A\ell}{6}\begin{bmatrix}2+\mu & 1-\mu & 0\\ 1-\mu & 4+2\mu & 1-\mu\\ 0 & 1-\mu & 2+\mu\end{bmatrix}\begin{bmatrix}\ddot{u}_{j-1}\\ \ddot{u}_j\\ \ddot{u}_{j+1}\end{bmatrix}+\frac{EA}{\ell}\begin{bmatrix}1 & -1 & 0\\ -1 & 2 & -1\\ 0 & -1 & 1\end{bmatrix}\begin{bmatrix}u_{j-1}\\ u_j\\ u_{j+1}\end{bmatrix}=0 \tag{9}$$

From this one takes the middle (node j) equation, which repeats in the infinite lattice

$$\frac{\rho A\ell}{6}\begin{bmatrix}1-\mu & 4+2\mu & 1-\mu\end{bmatrix}\begin{bmatrix}\ddot{u}_{j-1}\\ \ddot{u}_j\\ \ddot{u}_{j+1}\end{bmatrix}+\frac{EA}{\ell}\begin{bmatrix}-1 & 2 & -1\end{bmatrix}\times\begin{bmatrix}u_{j-1}\\ u_j\\ u_{j+1}\end{bmatrix}=0 \tag{10}$$

Evaluate Eq. (8) at $x=x_{j-1}=x_j-\ell$, $x=x_j$ and $x=x_{j+1}=x_j+\ell$ while keeping t continuous. Substitution into Eq. (10) gives the wave propagation condition

$$\frac{\rho A c_0^2}{3\ell}[6-(2+\mu)\Omega^2-(6-(1-\mu)\Omega^2)\cos\kappa]\times\left(\cos\frac{\Omega c_0 t}{\ell}-i\sin\frac{\Omega c_0 t}{\ell}\right)B=0 \tag{11}$$

If this is to vanish for any t and B, the expression in brackets must vanish. Solving gives the frequency to wave number relations

$$\Omega^2=\frac{6(1-\cos\kappa)}{2+\mu+(1-\mu)\cos\kappa}=\kappa^2+\frac{1-2\mu}{12}\kappa^4+\frac{1-10\mu+10\mu^2}{360}\kappa^6+\cdots$$

$$\kappa=\arccos\left[\frac{6-(2+\mu)\Omega^2}{6+(1-\mu)\Omega^2}\right]=\Omega-\frac{1-2\mu}{24}\Omega^3+\frac{9-20\mu+20\mu^2}{1920}\Omega^5+\cdots \tag{12}$$

Returning to physical wave number $k=\kappa/\ell$ and frequency $\omega=\Omega c_0/\ell$

$$\omega^2=\left(\frac{6c_0^2}{\ell^2}\right)\frac{1-\cos(k\ell)}{2+\mu+(1-\mu)\cos(k\ell)}=c_0^2k^2\left(1+\frac{1-2\mu}{12}k^2\ell^2+\frac{1-10\mu+10\mu^2}{360}k^4\ell^4+\cdots\right) \tag{13}$$

An equation that links frequency and wave number: $\omega=\omega(k)$ as in Eq. (13), is a *dispersion relation*. An oscillatory dynamical system is *nondispersive* if ω is linear in k, in which case $c=\omega/k$ is constant and the wave speed is the same for all frequencies. The dispersion relation for the continuum bar (within the limits of mechanics of materials assumptions) is $c_0=\omega_0/k_0$: all waves propagate with the same speed c_0. On the other hand the FEM model is *dispersive* for any μ, since from Eq. (12) we get

$$\frac{c}{c_0}=\frac{\omega}{kc_0}=\frac{1}{\kappa}\sqrt{\frac{6(1-\cos\kappa)}{2+\mu+(1-\mu)\cos\kappa}}=1+\frac{1-2\mu}{24}\kappa^2+\frac{1-20\mu+20\mu^2}{1920}\kappa^4+\cdots \tag{14}$$

The best fit to the continuum for *small wave numbers* $\kappa=k\ell\ll 1$ is obtained by taking $\mu=(1/2)$. This makes the second term of the foregoing series vanish. So from this standpoint the best mass matrix for the bar is

$$\mathbf{M}^e_{\mu}\big|_{\mu=(1/2)}=\frac{1}{2}\mathbf{M}^e_C+\frac{1}{2}\mathbf{M}^e_L=\frac{\rho A\ell}{12}\begin{bmatrix}5 & 1\\ 1 & 5\end{bmatrix} \tag{15}$$

Fig. 4(a) plots the dimensionless dispersion relation (12) for the consistent ($\mu=0$), diagonally lumped ($\mu=1$) and LC-averaged ($\mu=(1/2)$) mass matrices, along with the continuum-bar relation $\Omega_0=\kappa_0$. The lattice curves of Fig. 4(a) have a 2π period: $\Omega(\kappa)=\Omega(\kappa+2\pi n)$, n being an integer. Thus it is enough to plot $\Omega(\kappa)$ over $\kappa\in[0,2\pi]$. The maximum lattice frequency, which

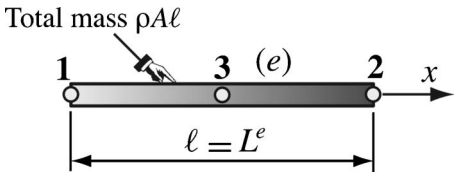

Fig. 5. The three-node prismatic bar element

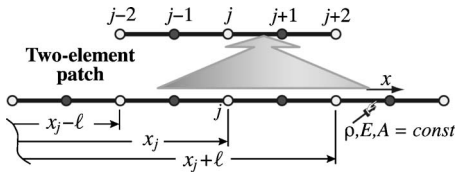

Fig. 6. Lattice of three-node bar elements from which a two-element patch is extracted

occurs for $\kappa=k\ell=\pi$ or $\lambda=2\ell$, is called the *Nyquist* or *folding frequency*.

If it is possible to pick μ as function of Ω or κ we can match the continuum over a certain range of κ or Ω. This can be done by equating $\Omega=\kappa$ (or $c=c_0$) and solving for μ

$$\begin{aligned}\mu_M &= 1+\frac{6}{\kappa^2}-\frac{3}{1-\cos\kappa}\\ &= \frac{1}{2}-\frac{\kappa^2}{40}-\frac{\kappa^4}{1{,}008}-\frac{\kappa^6}{28{,}800}-\cdots\\ &= \frac{1}{2}-\frac{4\pi^2\chi^2}{40}-\frac{16\pi^4\chi^4}{1{,}008}-\cdots\\ &= 1+\frac{6}{\Omega^2}-\frac{3}{1-\cos\Omega}\\ &= \frac{1}{2}-\frac{\Omega^2}{40}-\frac{\Omega^4}{1{,}008}-\frac{\Omega^6}{28{,}800}-\cdots\end{aligned} \tag{16}$$

in which $\chi=2\pi\kappa$. The function $\mu_M(\kappa)$ is plotted in Fig. 4(b). Interesting values are $\mu_M=0$ if $\kappa=3.38742306673364$ and $\mu_M=-(1/2)$ if $\kappa=\kappa_{\text{lim}}=4.05751567622863$. If $\kappa>\kappa_{\text{lim}}$ the fitted $\mathbf{M}^e$ becomes indefinite. So Eq. (16) is practically limited to the range $0\leqslant k\leqslant\approx 4/\ell$ as shown in the plot.

Best μ by Modified Equation

The gist of Fourier analysis is to find an exact solution, namely Eq. (8), which separates space and time in the characteristic equation (11). The rest is routine mathematics. The method of modified differential equations makes less initial assumptions but is not by any means routine. The objective is to find a modified differential equation that, if solved exactly, produces the FEM solution at nodes, and to compare it with the continuum wave equation given in Table 1. The optimal μ is the one that reproduces the original differential equation. For this simple element and a repeating lattice, this criterion leads to the same optimal mass matrix as Fourier analysis and is omitted to save space.

Three-Node Bar Element

As pictured in Fig. 5, this element is prismatic with length ℓ, cross-section area A, and mass density ρ. Midnode 3 is at the center. The element DOFs are arranged as $\mathbf{u}^e=[u_1\ u_2\ u_3]^T$. Its well known stiffness matrix is paired with a entry-weighted mass template

$$\mathbf{K}^e=\frac{EA}{3\ell}\begin{bmatrix}7 & 1 & -8\\ 1 & 7 & -8\\ -8 & -8 & 16\end{bmatrix}$$

$$\mathbf{M}^e_\mu=\frac{\rho A\ell}{90}\begin{bmatrix}12+\mu_1 & -3+\mu_3 & 6+\mu_4\\ -3+\mu_3 & 12+\mu_1 & 6+\mu_4\\ 6+\mu_4 & 6+\mu_4 & 48+\mu_2\end{bmatrix} \tag{17}$$

The idea behind the assumed form of $\mathbf{M}^e_\mu$ in Eq. (17) is to define the mass template as a parametrized deviation from the consistent mass matrix. That is, setting $\mu_1=\mu_2=\mu_3=\mu_4=0$ makes $\mathbf{M}^e_\mu=\mathbf{M}^e_C$. Setting $\mu_1=\mu_3=3$, $\mu_2=12$, and $\mu_4=-6$ gives the well known diagonally lumped mass matrix generated by Simpson's integration rule: $\mathbf{M}^e_L=\rho A\ell\ \mathbf{diag}[(1/6),(1/6),(2/3)]$. Thus again the standard models are template instances. Notice that $\mathbf{M}^e_\mu$ in Eq. (17) incorporates matrix and physical symmetries a priori but not conservation conditions.

Linear and angular momentum conservation requires $2\mu_1+\mu_2+2\mu_3+4\mu_4=0$ and $\mu_3=\mu_1$, respectively. Eliminating μ_3 and μ_4 from those constraints reduces the template to two parameters

$$\mathbf{M}^e_\mu=\frac{\rho A\ell}{360}\begin{bmatrix}4(12+\mu_1) & 4(-3+\mu_1) & 24-4\mu_1-\mu_2\\ 4(-3+\mu_1) & 4(12+\mu_1) & 24-4\mu_1-\mu_2\\ 24-4\mu_1-\mu_2 & 24-4\mu_1-\mu_2 & 4(48+\mu_2)\end{bmatrix} \tag{18}$$

For Eq. (18) to be nonnegative, $\mu_1\geqslant -9/2$ and $15+\mu_1-3\sqrt{5}\sqrt{9+2\mu_1}\leqslant(1/4)\mu_2\leqslant 15+\mu_1+3\sqrt{5}\sqrt{9+2\mu_1}$. These inequality constraints should be checked a posteriori.

Patch Equations

Unlike the two-node bar, two free parameters remain after the angular momentum conservation condition is enforced. Consequently we can ask for satisfactory wave propagation conditions in addition to conservation. To assess performance of mass-stiffness combinations we carry out the plane wave analysis of the infinite beam lattice shown in Fig. 6.

From the lattice we extract a typical two node patch as illustrated. The patch has five nodes: Three endpoints and two midpoints, which are assigned global numbers $j-2,\ j-1,\ldots,j+2$. The unforced semidiscrete dynamical equations of the patch are $\mathbf{M}^P\ddot{\mathbf{u}}^P+\mathbf{K}^P\mathbf{u}^P=\mathbf{0}$, where

J. Aerosp. Eng., 2006, 19(4): 241-258

$$\mathbf{M}^P = \frac{\rho A \ell}{360}\begin{bmatrix} 4(12+\mu_1) & 24-4\mu_1-\mu_2 & 4(-3+\mu_1) & 0 & 0 \\ 24-4\mu_1-\mu_2 & 4(48+\mu_2) & 24-4\mu_1-\mu_2 & 0 & 0 \\ 4(-3+\mu_1) & 24-4\mu_1-\mu_2 & 8(12+\mu_1) & 24-4\mu_1-\mu_2 & 4(-3+\mu_1) \\ 0 & 0 & 24-4\mu_1-\mu_2 & 4(48+\mu_2) & 24-4\mu_1-\mu_2 \\ 0 & 0 & 4(-3+\mu_1) & 24-4\mu_1-\mu_2 & 4(12+\mu_1) \end{bmatrix}$$

$$\mathbf{K}^P = \frac{EA}{3\ell}\begin{bmatrix} 7 & -8 & 1 & 0 & 0 \\ -8 & 16 & -8 & 0 & 0 \\ 1 & -8 & 14 & -8 & 1 \\ 0 & 0 & -8 & 16 & -8 \\ 0 & 0 & 1 & -8 & 7 \end{bmatrix} \tag{19}$$

$$\mathbf{u}^P = \begin{bmatrix} u_{j-2} & u_{j-1} & u_j & u_{j+1} & u_{j+2} \end{bmatrix}^T$$

From the foregoing we keep the third and fourth equations, namely those for nodes j and $j+1$. This selection provides the equations for a typical corner point j and a typical midpoint $j+1$. The retained patch equations are

$$\mathbf{M}^P_{j,j+1}\ddot{\mathbf{u}}_P + \mathbf{K}^P_{j,j+1}\mathbf{u}_P = \mathbf{0} \tag{20}$$

The 2×5 matrices $\mathbf{M}^P_{j,j+1}$ and $\mathbf{K}^P_{j,j+1}$ result on deleting rows one, two, and five of $\mathbf{M}^P$ and $\mathbf{K}^P$, respectively.

Fourier Analysis

We study the propagation of harmonic plane waves of wavelength λ, wave number $k=2\pi/\lambda$, and circular frequency ω over the lattice of Fig. 6. For convenience they are separated into corner and midpoint waves

$$u_c(x,t) = B_c e^{i(kx-\omega t)}, \quad u_m(x,t) = B_m e^{i(kx-\omega t)} \tag{21}$$

Wave $u_c(x,t)$ propagates only over corners and vanishes at midpoints, whereas $u_m(x,t)$ propagates only over midpoints and vanishes at corners. Both have the same wave number and frequency but different amplitudes and phases. [Waves (21) can be combined to form a single wave form that propagates over all nodes. The combination has two components that propagate with the same speed but in opposite directions. This is useful when studying boundary conditions or transitions in finite lattices, but is not needed for a periodic infinite lattice.] As in the two-node bar case, we will work with the dimensionless frequency $\Omega=\omega\ell/c_0$ and dimensionless wave number $\kappa=k\ell$.

Inserting Eq. (21) into Eq. (19), passing to dimensionless variables and requiring that solutions exist for any t yields the characteristic equation

$$\frac{1}{180}\begin{bmatrix} 960-2(48+\mu_2)\Omega^2 & -(960+(24-4\mu_1-\mu_2)\Omega^2)\cos\frac{1}{2}\kappa \\ \text{symm} & 4(210-(12+\mu_1)\Omega^2+(30+(3-\mu_1)\Omega^2)\cos\kappa) \end{bmatrix}\begin{bmatrix} B_c \\ B_m \end{bmatrix} = \mathbf{0} \tag{22}$$

For nontrivial solutions the determinant of the characteristic matrix must vanish. Solving for Ω^2 gives two frequencies for each wavenumber κ. They can be expressed as the dispersion relations

$$\Omega_a^2 = \frac{\phi_1+\delta}{\phi_5+\phi_6\cos\kappa}, \quad \Omega_o^2 = \frac{\phi_1-\delta}{\phi_5+\phi_6\cos\kappa} \tag{23}$$

in which $\phi_1=720[-208-\mu_2+(\mu_2-32)\cos\kappa]$, $\phi_2=64(\mu_1-60)\mu_1-32\mu_1\mu_2+13\mu_2^2+384(474+\mu_2)$, $\phi_3=12(-112+\mu_2)(128+\mu_2)$, $\phi_4=64[132+(\mu_1-60)\mu_1]-32(\mu_1-6)\mu_2+\mu_2^2$, $\phi_5=16[-540+(\mu_1-60)\mu_1]-8(30+\mu_1)\mu_2+\mu_2^2$, $\phi_6=2{,}880+16(\mu_1-60)\mu_1-8\mu_1\mu_2+\mu_2^2$, and $\delta=120\sqrt{6}\sqrt{\phi_2-\phi_3\cos\kappa-\phi_4\cos 2\kappa}$. Frequencies Ω_a and Ω_o pertain to the so-called *acoustic* and *optical* branches, respectively. This nomenclature originated in crystal physics, in which both branches have physical meaning as modeling molecular oscillations. (In molecular crystallography, acoustic waves are long-wavelength, low-frequency mechanical waves caused by sonic-like disturbances, in which adjacent molecules move in the same direction. Optical waves are short-wavelength, high-frequency oscillations caused by interaction with light or electromagnetics, in which adjacent molecules move in opposite directions. The last section provides references.)

Fig. 7 illustrates nomenclature used for a two-branched dispersion diagram such as that given by Eq. (23). The meaning of terms such as "stopping band" is defined in the following. In FEM discretization work only the acoustic branch has physical meaning because for small κ (i.e., long wavelengths) it approaches the continuum bar relation $\Omega=\kappa$, as shown in the next equation. On the other hand, the optical branch is physically spurious. It is caused by the discretization and pertains to high-frequency lattice oscillations, also known as "mesh modes."

The distinction between the two branches can be better grasped by examining the Taylor expansions of frequencies (23) about $\kappa=0$

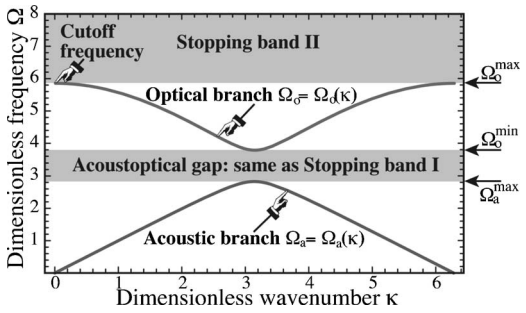

Fig. 7. Notation pertaining to a typical two-branch dispersion diagram. The stopping band is the union of I and II.

$$\Omega_a^2 = \kappa^2 + \frac{C_4\kappa^4}{4!} + \frac{C_6\kappa^6}{6!} + \frac{C_8\kappa^8}{8!} + \cdots, \quad \Omega_o^2 = D_0 + \frac{D_2\kappa^2}{2!} + \cdots$$

$$5 \times 1{,}440C_4 = 14{,}400 - \psi_1^2 = (240 - 4\mu_1 + \mu_2)(4\mu_1 - \mu_2)$$

$$10 \times 1{,}440^2 C_6 = 41{,}472{,}000 + 7{,}200\psi_1^2 + 180\psi_1^3 + \psi_1^4 - 720\psi_1^2\psi_2$$

$$60 \times 1{,}440^3 C_8 = -2{,}030{,}469{,}120{,}000 + 348{,}364{,}800\psi_1^2 - 14{,}515{,}200\psi_1^3 - 342{,}720\psi_1^4 - 2{,}520\psi_1^5 - 7\psi_1^6 + 58{,}060{,}800\psi_1^2\psi_2 + 1{,}451{,}520\psi_1^3\psi_2 + 10{,}080\psi_1^4\psi_2 - 2{,}903{,}040\psi_1^2\psi_2^2$$

$$D_0 = \frac{1}{\psi_3}, \quad D_2 = -\frac{\psi_1^2(43{,}200 + 360\psi_1 + \psi_1^2 - 1{,}440\psi_2)}{\psi_3^2} \quad (24)$$

Here $\psi_1 = 4\mu_1 - \mu_2 - 120$, $\psi_2 = \mu_1 - 2$, and $\psi_3 = 28{,}800 + 360\psi_1 + \psi_1^2 - 1{,}440\psi_2 = -2{,}880 - 960\mu_1 + 16\mu_1^2 - 120\mu_2 - 8\mu_1\mu_2 + \mu_2^2$. Note that the expansion of Ω_a^2 approaches κ^2 as $\kappa \to 0$. Clearly the acoustic branch is the long-wavelength counterpart of the continuum bar, for which $\Omega = \kappa$. On the other hand, the optical branch has a nonzero frequency $\Omega_o^2 = 1/\psi_3$ at $\kappa = 0$, called the *cutoff frequency*, which cannot vanish although it may go to infinity if $\psi_3 = 0$. As illustrated in Fig. 7, the lowest and highest values of Ω_o (taking the + square root of Ω_o^2) are called Ω_o^{max} and Ω_o^{min}, respectively, whereas the largest Ω_a is called Ω_a^{max}. Usually, but not always, Ω_0^{min} and Ω_a^{max} occur at $\kappa = \pi$.

If $\Omega_o^{min} > \Omega_a^{max}$, the range $\Omega_o^{min} > \Omega > \Omega_a^{max}$ is called the *acoustoptical frequency gap*. Frequencies in this gap are said to pertain to Portion I of the *stopping band*, a term derived from filter technology. Frequencies $\Omega > \Omega_o^{max}$ pertain to Portion II of the stopping band. A stopping band frequency cannot be propagated as harmonic plane wave over the lattice. This can be proven by showing that if Ω pertains to the stopping band, the characteristic equation (22) has complex roots with nonzero real parts. This causes exponential attenuation so any disturbance with that frequency will decay exponentially.

Customization

Fig. 8 shows dispersion curves for the four parameter settings tabulated in Table 2. The four associated mass matrices are positive definite. Dispersion curves for the consistent mass $\mathbf{M}_C^e$ and the diagonally lumped mass $\mathbf{M}_L^e$ are shown in Figs. 8(a and b). Both matrices have an acoustical branch that agrees with the continuum to order $O(\kappa^4)$, as shown by the series listed in Table 2.

For a mass matrix to produce fourth order accuracy in the acoustic branch, $C_4 = 0$ in series (24). This has the two solutions $\mu_2 = 4\mu_1$ and $\mu_2 = 4\mu_1 - 240$. Both CM and DLM comply with the first solution. To get sixth order accuracy for small κ we impose $C_4 = C_6 = 0$. This has only two solutions: $\{\mu_1 = 2, \mu_2 = 8\}$ and $\{\mu_1 = 62, \mu_2 = 8\}$. Only the first solution is of interest, as the second one produces large positive-negative entries and exactly the

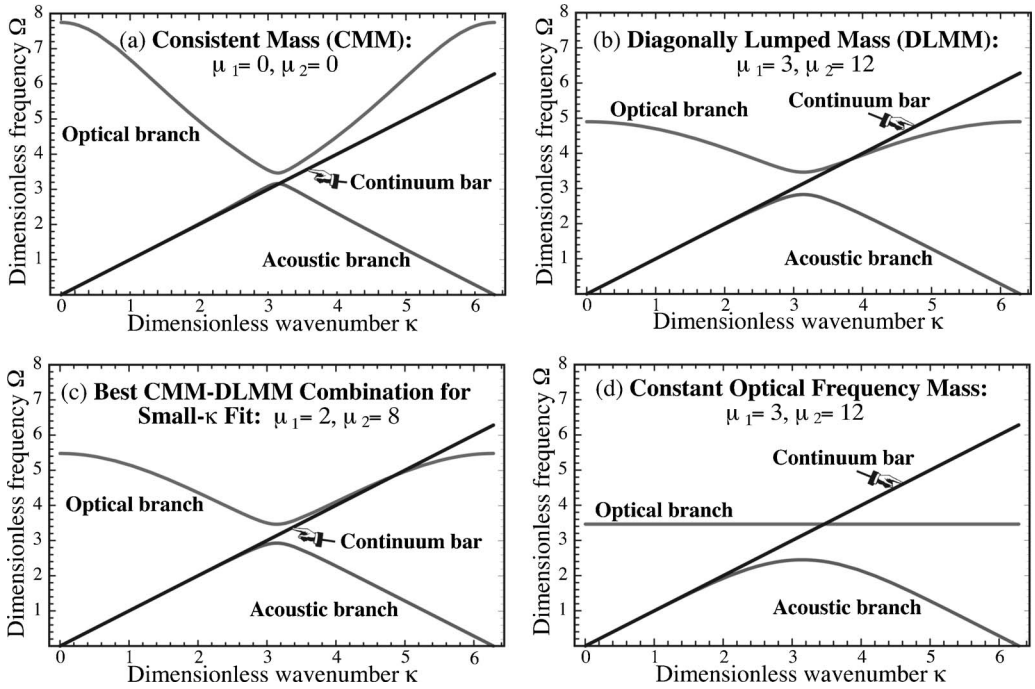

Fig. 8. Dispersion curves of four mass matrices for the three-node prismatic bar, plotted for $\kappa \in [0, 2\pi]$. Plots display acoustic branch, optical branch and continuum-bar line $\Omega = \kappa$. Acoustic and optical branches repeat with period 2π; note symmetry about $\kappa = \pi$.

J. Aerosp. Eng., 2006, 19(4): 241-258

Table 2. Useful Mass Matrices for Three-Node Bar Element

Mass matrix	Template signature μ_1	μ_2	μ_3	μ_4	Taylor expansion of Ω_a^2 (acoustic branch)	Taylor expansion of Ω_a^2 (optical branch)
CMM	0	0	0	0	$\kappa^2+\frac{\kappa^6}{720}-\frac{11\kappa^8}{151{,}200}+\frac{7\kappa^{10}}{129{,}600}+O(\kappa^{12})$	$60-20\kappa^2+O(\kappa^4)$
DLMM	3	12	3	−6	$\kappa^2-\frac{\kappa^6}{1{,}440}-\frac{\kappa^8}{48{,}383}-\frac{\kappa^{10}}{4{,}147{,}200}+O(\kappa^{12})$	$24-2\kappa^2+O(\kappa^4)$
BLC	2	8	2	−4	$\kappa^2-\frac{\kappa^8}{37{,}800}-\frac{\kappa^{10}}{864{,}000}+O(\kappa^{12})$	$30-\frac{15\kappa^2}{4}+O(\kappa^4)$
COF	8	32	8	−16	$\kappa^2-\frac{\kappa^6}{240}-\frac{\kappa^8}{6{,}048}+\frac{\kappa^{10}}{86{,}400}O+O(\kappa^{12})$	12

same dispersion curves. The resulting mass matrix turns out to be a linear combination of CMM and DLMM. It is labeled BLC for "best lumped-consistent combination"

$$\mathbf{M}^e_{\mathrm{BLC}}=\frac{\rho A\ell}{90}\begin{bmatrix}14&-1&2\\-1&14&2\\2&2&56\end{bmatrix}=\frac{1}{3}\mathbf{M}^e_C+\frac{2}{3}\mathbf{M}^e_L \tag{25}$$

As shown in Table 2, the acoustic branch of this matrix agrees up to $O(\kappa^6)$ with the continuum bar. The dispersion curves are shown in Fig. 8(c).

A different kind of customization is advisable in dynamic simulations that involve propagation of high frequencies, such as shock and impact. The presence of the optical branch is undesirable, because it introduces spurious noise into the solutions. For such problems the two-node bar, which lacks an optical branch, should be used. If use of a three-node model is mandated for some reason, the harmful effects of the optical branch can be reduced by making it of constant frequency. Setting $\{\mu_1=8, \mu_2=32\}$ produces the mass

$$\mathbf{M}^e_{\mathrm{COF}}=\frac{\rho A\ell}{90}\begin{bmatrix}10&5&-10\\5&10&-10\\-10&-10&80\end{bmatrix} \tag{26}$$

in which acronym COF stands for "constant optical frequency." Then $\Omega_o^2=12$ for all wave numbers, as pictured in Fig. 8(d). This configuration maximizes the stopping band and facilitates the implementation of a narrow band filter centered at that frequency. The acoustic branch accuracy is inferior to that of the other models, however, so this customization involves a tradeoff.

One final parameter choice is worth mentioning as a curiosity. Setting $\{\mu_1=-2,\mu_2=-8\}$ produces a dispersion diagram *with no stopping band*: The optical branch comes down from $+\infty$ at $\kappa=0,2\pi$ and merges with the acoustic branch at $\kappa=\pi$. The application of this mass matrix (which is singular) as a modeling tool is presently unclear and its dispersion diagram is omitted.

Two-Node Timoshenko Beam Element

The last example is far more elaborate than the previous two. The goal is to construct a mass template for the prismatic, plane-beam Timoshenko model. This includes the Bernoulli-Euler model as special case, and consequently results can be reused for that model. The continuum Timoshenko model is first examined in some detail, since frequency expansion formulas applicable to template customization by characteristic root fitting are not easily found in the literature.

Continuum Analysis

Consider a structural beam member modeled as a shear-flexible Timoshenko plane beam, as illustrated in Fig. 9. Fig. 9 provides the notation used in the following. Section properties $\{\rho,E,A,A_s,I,I_R\}$ are constant along x. The beam is transversally loaded by line load $q(x,t)$ (not shown in Fig. 9), with dimension of force per length. The primary kinematic variables are the transverse deflection $v(x,t)$ and the total cross-section rotation $\theta(x,t)=v'(x,t)+\gamma(x,t)$, where $\gamma=V/(GA_s)$ is the mean shear rotation. The kinetic and potential energies in terms of those variables are

$$T[v,\theta]=\frac{1}{2}\int_0^L(\rho A\dot{v}^2+\rho I_R\dot{\theta}^2)dx$$

$$\Pi[v,\theta]=\int_0^L\left(\frac{1}{2}EI(v'')^2+\frac{1}{2}GA_s(\theta-v')^2-qv\right)dx \tag{27}$$

where superposed dots denote time derivatives. The equations of motion (EOM) follow on forming the Euler-Lagrange equations from the Lagrangian $L=T-\Pi$:

$$\frac{\delta L}{\delta v}=0\rightarrow GA_s(\theta'-v'')+\rho A\ddot{v}=q$$

$$\frac{\delta L}{\delta\theta}=0\rightarrow EI\theta''+GA_s(v'-\theta)-\rho I_R\ddot{\theta}=0 \tag{28}$$

An expedient way to eliminate θ is to rewrite the two equations in Eq. (28) in transform space

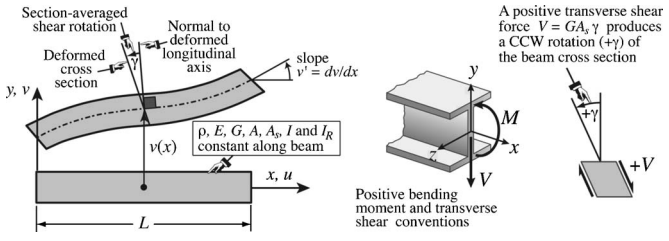

Fig. 9. A plane beam member modeled as Timoshenko beam, illustrating notation followed in the continuum analysis. Transverse load $q(x)$ not shown to reduce clutter. Infinitesimal deflections and deformations grossly exaggerated for visibility.

$$\begin{bmatrix} \rho A s^2 - GA_s p^2 & GA_s p \\ GA_s p & EIp^2 - GA_s - \rho I_R s^2 \end{bmatrix} \begin{bmatrix} \tilde{v} \\ \tilde{\theta} \end{bmatrix} = \begin{bmatrix} \tilde{q} \\ 0 \end{bmatrix} \quad (29)$$

in which $\{p, s, \tilde{v}, \tilde{\theta}, \tilde{q}\}$ denote transforms of $\{d/dx, d/dt, v, \theta, q\}$, respectively (Fourier in x and Laplace in t). Eliminating $\tilde{\theta}$ and returning to the physical domain yields

$$EIv'''' + \rho A\ddot{v} - \left(\rho I_R + \frac{\rho AEI}{GA_s}\right)\ddot{v}'' + \frac{\rho^2 AI_R}{GA_s}\ddot{\ddot{v}} = q - \frac{EI}{GA_s}q'' + \frac{\rho I_R}{GA_s}\ddot{q} \quad (30)$$

(Note that this derivation does not presume that $I \equiv I_R$, as usually done in textbooks.) For the unforced case $q=0$, Eq. (30) has plane wave solutions $v = B\exp[i(k_0 x - \omega_0 t)]$. The propagation condition yields a characteristic equation relating k_0 and ω_0. To render it dimensionless, introduce a reference phase velocity $c_0^2 = EI/(\rho AL^4)$ so that $k_0 = \omega_0/c_0 = 2\pi/\lambda_0$, a dimensionless frequency $\Omega = \omega_0 L/c_0$ and a dimensionless wave number $\kappa = k_0 L$. As dimensionless measures of relative bending-to-shear rigidities and rotary inertia take

$$\Phi_0 = 12EI/(GA_s L^2), \quad r_R^2 = I_R/A, \quad \Psi_0 = r_R/L \quad (31)$$

The resulting dimensionless characteristic equation is

$$\kappa^4 - \Omega^2 - \left(\frac{1}{12}\Phi_0 + \Psi_0^2\right)\kappa^2\Omega^2 + \frac{1}{12}\Phi_0\Psi_0^2\,\Omega^4 = 0 \quad (32)$$

This is quadratic in Ω^2. Its solution yields two kinds of squared-frequencies, which will be denoted by Ω_f^2 and Ω_s^2 because they are associated with flexural and shear modes, respectively. Their expressions are listed in the following along with their small-κ (long wavelength) Taylor series:

$$\begin{aligned} \Omega_f^2 &= 6\frac{P - \sqrt{Q}}{\Phi_0\Psi_0^2} \\ &= \kappa^4 - \left(\frac{1}{12}\Phi_0 + \Psi_0^2\right)\kappa^6 + \left(\frac{1}{144}\Phi_0^2 + \frac{1}{4}\Phi_0\Psi_0^2 + \Psi_0^4\right)\kappa^8 \\ &\quad - \left(\frac{1}{1728}\Phi_0^3 + \frac{1}{24}\Phi_0^2\Psi_0^2 + \frac{1}{2}\Phi_0\Psi_0^4 + \Psi_0^6\right)\kappa^{10} + \cdots \\ &= \kappa^4 + A_6\kappa^6 + A_8\kappa^8 + \cdots \end{aligned} \quad (33)$$

$$\begin{aligned} \Omega_s^2 &= 6\frac{P + \sqrt{Q}}{\Phi_0\Psi_0^2} \\ &= \frac{12}{\Phi_0\Psi_0^2} + \left(\frac{12}{\Phi_0} + \frac{1}{\Psi_0^2}\right)\kappa^2 - \kappa^4 + \left(\frac{1}{12}\Phi_0 + \Psi_0^2\right)\kappa^6 + \cdots \\ &= B_0 + B_2\kappa^2 + \cdots \end{aligned} \quad (34)$$

in which $P = 1 + \kappa^2[\Psi_0^2 + (1/12)\Phi_0]$ and $Q = P^2 - (1/3)\kappa^4\Phi_0\Psi_0^2$. The dispersion relation $\Omega_f^2(\kappa)$ defines the *flexural frequency branch* whereas $\Omega_s^2(\kappa)$ defines the *shear frequency branch*. If $\Phi_0 \to 0$ and $\Psi_0 \to 0$, which reduces the Timoshenko model to the Bernoulli-Euler one, Eq. (32) collapses to $\Omega^2 = \kappa^4$ or (in principal value) $\Omega = \kappa^2$. This surviving branch pertains to flexural motions whereas the shear branch disappears—or more precisely, $\Omega_s^2(\kappa) \to +\infty$. It is easily shown that the radicand Q in the exact expressions is strictly positive for any $\{\Phi_0 > 0, \Psi_0 > 0, \kappa \geq 0\}$. Thus for any such triple, Ω_f^2 and Ω_s^2 are real, finite and distinct with $\Omega_f^2(\kappa) < \Omega_s^2(\kappa)$; further, $\{\Omega_f^2, \Omega_s^2\}$ increase indefinitely as $\kappa \to \infty$. Following the nomenclature introduced in Fig. 7, the value Ω_s at $\kappa = 0$ is called the cutoff frequency.

To see how branches look, consider a beam of a narrow rectangular cross section of width b and height h, fabricated of isotropic material with Poisson's ratio ν. We have $E/G = 2(1+\nu)$ and $A_s/A \approx 5/6$. [Actually a more refined A_s/A ratio would be $10(1+\nu)/(12+11\nu)$, but that makes little difference in the results.] In addition $A = bh$, $I = I_R = bh^3/12$, $r_R^2 = I_R/A = h^2/12$, $\Psi_0^2 = r_R^2/L^2 = (1/12)h^2/L^2$ and $\Phi_0 = 12EI/(GA_sL^2) = 12(1+\nu)h^2/(5L^2)$. As $\Phi_0/12 = 12(1+\nu)\,\Psi_0^2/5$, the first-order effect of shear on Ω_f^2, as measured by the κ^6 term in Eq. (33), is 2.4–3.6 times that from rotary inertia, depending on ν. Replacing into Eqs. (33) and (34) yields

$$\begin{aligned} \left.\begin{matrix} \Omega_f^2 \\ \Omega_s^2 \end{matrix}\right\} &= \frac{60 + \kappa^2(17+12\nu)\Lambda^2 \mp \sqrt{(60+\kappa^2(17+12\nu)\Lambda^2)^2 - 240\kappa^4(1+\nu)\Lambda^4}}{2(1+\nu)\Lambda^4} \\ &= \begin{cases} \kappa^4 - \dfrac{1}{60}(17+12\nu)\Lambda^2\kappa^6 + \dfrac{1}{3600}(349+468\nu+144\nu^2)\Lambda^4\kappa^8 + \cdots \\ \dfrac{60 + (17+12\nu)\Lambda^2\kappa^2 - (1+\nu)\Lambda^4\kappa^4 + \cdots}{(1+\nu)\Lambda^4} \end{cases} \end{aligned} \quad (35)$$

in which $\Lambda = h/L$. Dispersion curves $\Omega(\kappa)$ for $\Lambda = h/L = (1/4)$ and $\nu = \{0, (1/2)\}$ are plotted in Fig. 10(a). Phase velocities Ω/κ are shown in Fig. 10(b). Fig. 10(b) also shows the flexural branch of the Bernoulli-Euler model. The phase velocities of the Timoshenko model tend to finite values in the shortwave, high-frequency limit $\kappa \to \infty$, which is physically correct. The Bernoulli-Euler model is wrong in that limit because it predicts an infinite propagation speed.

J. Aerosp. Eng., 2006, 19(4): 241-258

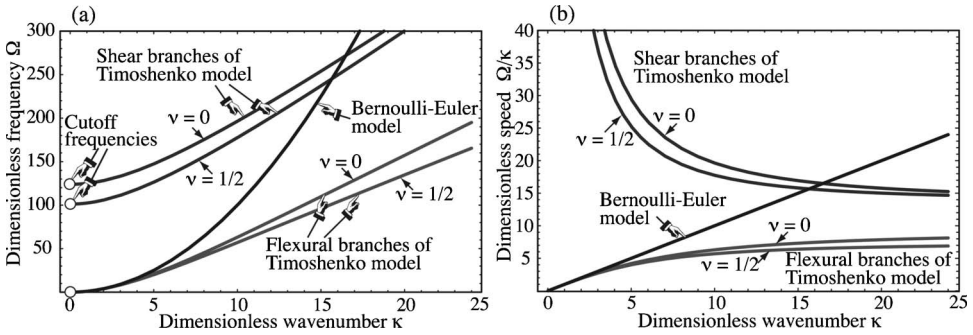

Fig. 10. Spectral behavior of continuum Timoshenko beam model for a narrow $b \times h$ rectangular cross-section. (a) Dispersion curves $\Omega(\kappa)$ for $\Lambda = h/\ell = 1/4$ and two Poisson's ratios; showing Timoshenko flexural and shear branches and Bernoulli-Euler curve $\Omega = \kappa^2$. (b) Wave speed Ω/κ.

Beam Element

The shear-flexible plane beam member of Fig. 9 is discretized by two-node elements. An individual element of this type is shown in Fig. 11, which illustrates its kinematics. The element has four nodal freedoms arranged as

$$\mathbf{u}^e = [v_1 \quad \theta_1 \quad v_2 \quad \theta_2]^T \tag{36}$$

Here $\theta_1 = v_1 + \gamma_1$ and $\theta_2 = v_2 + \gamma_2$ are the total cross-section rotations evaluated at the end nodes. The dimensionless properties (31) that characterize relative shear rigidity and rotary inertia are redefined using the element length

$$\Phi = 12EI/(GA_s\ell^2), \quad r_R^2 = I_R/A, \quad \Psi = r_R/\ell \tag{37}$$

If the beam member is divided into N_e elements of equal length, $\ell = L/N_e$ whence $\Phi = \Phi_0 N_e^2$ and $\Psi = \Psi_0 N_e$. Thus even if Φ_0 and Ψ_0 are small with respect to one, they can grow without bound as the mesh is refined. For example if $\Phi_0 = 1/4$ and $\Psi_0^2 = 1/100$, which are typical values for a moderately thick beam, and we take $N_e = 32$, then $\Phi \approx 250$ and $\Psi^2 \approx 10$. Those are no longer small numbers, a fact that will impact performance as N_e increases. The stiffness matrix to be paired with the mass template is taken to be that of the equilibrium element

$$\mathbf{K}^e = \frac{EI}{\ell^3(1+\Phi)} \begin{bmatrix} 12 & 6\ell & -12 & 6\ell \\ 6\ell & \ell^2(4+\Phi) & -6\ell & \ell^2(2-\Phi) \\ -12 & -6\ell & 12 & -6\ell \\ 6\ell & \ell^2(2-\Phi) & -6\ell & \ell^2(4+\Phi) \end{bmatrix} \tag{38}$$

This is known to be nodally exact in static analysis for a prismatic beam member, and therefore an optimal choice in that sense.

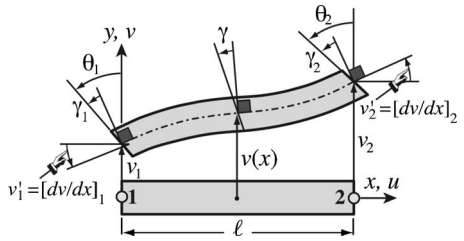

Fig. 11. Two-node element for Timoshenko plane beam, illustrating kinematics. As in Fig. 9, displacements and rotations are grossly exaggerated for visibility.

Setting Up the Mass Template

FEM derivations usually split the 4×4 mass matrix of this element into $\mathbf{M}^e = \mathbf{M}_v^e + \mathbf{M}_\theta^e$, where $\mathbf{M}_v^e$ and $\mathbf{M}_\theta^e$ come from the translational inertia and rotary inertia terms, respectively, of the kinetic energy functional $T[v, \theta]$ of Eq. (27). The most general mass template would result from applying a entry-weighted parametrization of those two matrices. This would require a set of 20 parameters (10 in each matrix), reducible to about one half on account of invariance and conservation conditions. Attacking the problem this way, however, leads to unwieldy algebraic equations even with the help of a computer algebra system, while concealing the underlying physics. A divide and conquer approach works better. This is briefly outlined next and covered in more detail in the next subsections.

(I) Express $\mathbf{M}^e$ as the one-parameter matrix-weighted form $\mathbf{M}^e = (1-\mu_0)\mathbf{M}_F^e + \mu_0 \mathbf{M}_D^e$. Here $\mathbf{M}_F^e$ is full and includes the CMM as instance, whereas $\mathbf{M}_D^e$ is 2×2 block diagonal and includes the DLMM as instance. This is plainly a generalization of the LC linear combination (2).

(II) Decompose the foregoing mass components as $\mathbf{M}_F^e = \mathbf{M}_{FT}^e + \mathbf{M}_{FR}$ and $\mathbf{M}_D^e = \mathbf{M}_{DT}^e + \mathbf{M}_{DR}^e$, where subscripts identify their source in the kinetic energy functional: T if coming from the translational inertia term $(1/2)\rho A\dot{v}^2$ and R from the rotary inertia term $(1/2)\rho I_R \dot{\theta}^2$.

(III) Both components of $\mathbf{M}_F^e$ are expressed as parametrized spectral forms, whereas those of $\mathbf{M}_D^e$ are expressed as entry weighted. The main reasons for choosing spectral forms for the full matrix are reduction of parameters and physical transparency. No such concerns apply to $\mathbf{M}_D^e$.

The analysis follows a "bottom up" sequence, in order (III)–(II)–(I). This has the advantage that if a satisfactory custom mass matrix for a target application emerges during (III), Stages (II) and (I) need not be carried out, and that matrix directly used by setting the remaining parameters to zero.

Full-Mass Parametrization

As noted earlier, one starts with full-matrix spectral forms. Let ξ denote the natural coordinate that varies from -1 at node 1 to $+1$ at node 2. Two element transverse displacement expansions in generalized coordinates are introduced

$$v_T(\xi) = L_1(\xi)c_{T1} + L_2(\xi)c_{T2} + L_3(\xi)c_{T3} + L_4(\xi)c_{T4} = \mathbf{L}_T\mathbf{c}_T$$

$$v_R(\xi) = L_1(\xi)c_{R1} + L_2(\xi)c_{R2} + L_3(\xi)c_{R3} + \hat{L}_4(\xi)c_{R4} = \mathbf{L}_R\mathbf{c}_R$$

$$L_1(\xi)=1,\ L_2(\xi)=\xi,\ L_3(\xi)=\frac{1}{2}(3\xi^2-1),\ L_4(\xi)=\frac{1}{2}(5\xi^3-3\xi)$$

$$\widehat{L}_4(\xi)=\frac{1}{2}(5\xi^3-(5+10\Phi)\xi)=L_4(\xi)-(1+5\Phi)\xi \tag{39}$$

The v_T and v_R expansions are used for the translational and rotational parts of the kinetic energy, respectively. The interpolation function set $\{L_i\}$ used for v_T is formed by the first four Legendre polynomials over $\xi=[-1,1]$. The set used for v_R is the same except that L_4 is adjusted to $\widehat{L}_4$ to produce a diagonal rotational mass matrix. All amplitudes c_{Ti} and c_{Ri} have dimension of length.

Unlike the usual Hermite cubic shape functions, the polynomials in Eq. (39) have a direct physical interpretation. L_1=translational rigid mode; L_2=rotational rigid mode; L_3=pure-bending mode symmetric about $\xi=0$; L_4 and $\widehat{L}_4$=bending-with-shear modes antisymmetric about $\xi=0$.

With the usual abbreviation $(\cdot)'\equiv d(\cdot)/dx=(2/\ell)d(\cdot)/d\xi$, the associated cross-section rotations are

$$\theta_T=v_T'+\gamma_T=\mathbf{L}_T'\mathbf{c}_T+\gamma_T,\quad \theta_R=v_R'+\gamma_R=\mathbf{L}_R'\mathbf{c}_R+\gamma_R \tag{40}$$

in which the mean shear distortions are constant over the element

$$\gamma_T=\frac{\Phi\ell^2}{12}v_T'''=\frac{10\Phi}{\ell}c_{T4},\quad \gamma_R=\frac{\Phi\ell^2}{12}v_R'''=\frac{10\Phi}{\ell}c_{R4} \tag{41}$$

The kinetic energy of the element in generalized coordinates is

$$\begin{aligned}T^e&=\frac{1}{2}\int_0^\ell(\rho A\dot{v}_T^2+\rho I_R\dot{\theta}_R^2)dx\\&=\frac{\ell}{4}\int_{-1}^1(\rho A\dot{v}_T^2+\rho I_R\dot{\theta}_R^2)d\xi\\&=\frac{1}{2}\dot{\mathbf{c}}_T^T\mathbf{D}_T\dot{\mathbf{c}}_T+\frac{1}{2}\dot{\mathbf{c}}_R^T\mathbf{D}_R\dot{\mathbf{c}}_R,\end{aligned} \tag{42}$$

in which both generalized mass matrices turn out to be diagonal as intended

$$\mathbf{D}_T=\rho A\,\ell\ \mathbf{diag}\left[1\quad\frac{1}{3}\quad\frac{1}{5}\quad\frac{1}{7}\right]$$

$$\mathbf{D}_R=4\rho A\,\ell\,\Psi^2\,\mathbf{diag}[0\quad 1\quad 3\quad 5]$$

To convert $\mathbf{D}_T$ and $\mathbf{D}_R$ to physical coordinates (36), v_T, v_R, θ_T, and θ_R are evaluated at the nodes by setting $\xi=\pm1$. This establishes the transformations $\mathbf{u}^e=\mathbf{G}_T\mathbf{c}_T$ and $\mathbf{u}^e=\mathbf{G}_R\mathbf{c}_R$. Inverting: $\mathbf{c}_T=\mathbf{H}_T\mathbf{u}^e$ and $\mathbf{c}_R=\mathbf{H}_R\mathbf{u}^e$ with $\mathbf{H}_T=\mathbf{G}_T^{-1}$ and $\mathbf{H}_R=\mathbf{G}_R^{-1}$. A symbolic calculation yields

$$\mathbf{H}_T=\frac{1}{60(1+\Phi)}\begin{bmatrix}30(1+\Phi)&5\ell(1+\Phi)&30(1+\Phi)&-5\ell(1+\Phi)\\-36-30\Phi&-3\ell&36+30\Phi&-3\ell\\0&-5\ell(1+\Phi)&0&5\ell(1+\Phi)\\6&3\ell&-6&3\ell\end{bmatrix}$$

$$\mathbf{H}_R=\frac{1}{60(1+\Phi)}\begin{bmatrix}30(1+\Phi)&5\ell(1+\Phi)&30(1+\Phi)&-5\ell(1+\Phi)\\-30&15\ell\Phi&30&15\ell\Phi\\0&-5\ell(1+\Phi)&0&5\ell(1+\Phi)\\6&3\ell&-6&3\ell\end{bmatrix} \tag{43}$$

Matrices $\mathbf{H}_T$ and $\mathbf{H}_R$ differ only in the second row. This comes from the adjustment of L_4 to $\widehat{L}_4$ in Eq. (39). To render this into a spectral template inject six free parameters in the generalized masses while moving $4\Psi^2$ inside $\mathbf{D}_{R\mu}$

$$\mathbf{D}_{T\mu}=\rho A\,\ell\ \mathbf{diag}\left[1\quad\frac{1}{3}\mu_{T1}\quad\frac{1}{5}\mu_{T2}\quad\frac{1}{7}\mu_{T3}\right]$$

$$\mathbf{D}_{R\mu}=\rho A\,\ell\ \mathbf{diag}[0\quad\mu_{R1}\quad 3\mu_{R2}\quad 5\mu_{R3}] \tag{44}$$

The transformation matrices (43) are reused without change to produce $\mathbf{M}_F^e=\mathbf{H}_T^T\mathbf{D}_{T\mu}\mathbf{H}_T+\mathbf{H}_R^T\mathbf{D}_{R\mu}\mathbf{H}_R$. If $\mu_{T1}=\mu_{T2}=\mu_{T3}=1$ and $\mu_{R1}=\mu_{R2}=\mu_{R3}=4\Psi^2$ one obtains the well known CMM of Archer (1963), see Przemieniecki (1968, p. 296), as a valuable check. Configuration (44) already accounts for linear momentum conservation, which is why the upper diagonal entries are not parametrized. Imposing also angular momentum conservation requires $\mu_{T1}=1$ and $\mu_{R1}=4\Psi^2$, whence the template is reduced to four parameters

$$\begin{aligned}\mathbf{M}_F^e=\rho A\,\ell\,\mathbf{H}_T^T&\begin{bmatrix}1&0&0&0\\0&\frac{1}{3}&0&0\\0&0&\frac{1}{5}\mu_{T2}&0\\0&0&0&\frac{1}{7}\mu_{T3}\end{bmatrix}\mathbf{H}_T\\+\rho A\,\ell\,\mathbf{H}_R^T&\begin{bmatrix}0&0&0&0\\0&4\Psi^2&0&0\\0&0&3\mu_{R2}&0\\0&0&0&5\mu_{R3}\end{bmatrix}\mathbf{H}_R\end{aligned} \tag{45}$$

Because both $\mathbf{H}_T$ and $\mathbf{H}_R$ are nonsingular, choosing all four parameters in Eq. (45) to be nonnegative guarantees that $\mathbf{M}_F^e$ is nonnegative. This useful property eliminates lengthy *a posteriori*

J. Aerosp. Eng., 2006, 19(4): 241-258

checks. Setting $\mu_{T2}=\mu_{T3}=\mu_{R2}=\mu_{R3}=0$ and $\Phi=0$ yields the correct mass matrix for a rigid beam, including rotary inertia. This simple result highlights the physical transparency of spectral forms.

Block-Diagonal Mass Parametrization

Template (45) has a flaw: It does not include the DLMM. To remedy the omission, a block diagonal form, with four free parameters: $\{\nu_{T1},\nu_{T2},\nu_{R1},\nu_{R2}\}$ is separately constructed

$$\mathbf{M}_D^e=\mathbf{M}_{DT}+\mathbf{M}_{DR}$$
$$=\rho A\,\ell\begin{bmatrix}\frac{1}{2} & \nu_{T1}\,\ell & 0 & 0\\ \nu_{T1}\,\ell & \nu_{T2}\ell^2 & 0 & 0\\ 0 & 0 & \frac{1}{2} & -\nu_{T1}\ell\\ 0 & 0 & -\nu_{T1}\,\ell & \nu_{T2}\ell^2\end{bmatrix}$$
$$+\rho A\,\ell\begin{bmatrix}0 & \nu_{R1}\,\ell & 0 & 0\\ \nu_{R1}\,\ell & \nu_{R2}\ell^2 & 0 & 0\\ 0 & 0 & 0 & -\nu_{R1}\ell\\ 0 & 0 & -\nu_{R1}\,\ell & \nu_{R2}\ell^2\end{bmatrix} \tag{46}$$

Four parameters can be merged into two by adding

$$\mathbf{M}_D^e=\rho A\,\ell\begin{bmatrix}\frac{1}{2} & \nu_1\,\ell & 0 & 0\\ \nu_1\,\ell & \nu_2\ell^2 & 0 & 0\\ 0 & 0 & \frac{1}{2} & -\nu_1\ell\\ 0 & 0 & -\nu_1\,\ell & \nu_2\ell^2\end{bmatrix} \tag{47}$$

where $\nu_1=\nu_{T1}+\nu_{R1}$ and $\nu_2=\nu_{T2}+\nu_{R2}$. Sometimes it is convenient to use the split form (46), for example in lattices with varying beam properties or lengths, a topic not considered there. Otherwise Eq. (47) suffices. If $\nu_1=0$, $\mathbf{M}_D^e$ is diagonal. However for computational purposes a block diagonal form is just as good and provides additional customization power. Terms in the (1,1) and (3,3) positions must be as shown to satisfy linear momentum conservation. If angular momentum conservation is imposed a priori it is necessary to set $\nu_2=(1/2)\Psi^2$, and only one parameter remains.

The general template is obtained as a linear combination of $\mathbf{M}_F^e$ and $\mathbf{M}_D^e$

$$\mathbf{M}^e=(1-\mu_0)\mathbf{M}_F^e+\mu_0\mathbf{M}_D^e \tag{48}$$

Summarizing, there is a total of seven parameters to play with: Four in $\mathbf{M}_F^e$, two in $\mathbf{M}_D^e$, plus μ_0. This is less that the 9-to-11 that would result from a full entry-weighted parametrization, so not all possible mass matrices are included by (48).

Fourier Analysis

An infinite lattice of identical beam elements of length ℓ is set up. Plane waves of wave number k and frequency ω propagating over the lattice are represented by

$$v(x,t)=B_v\exp[i(kx-\omega t)],\quad \theta(x,t)=B_\theta\exp[i(kx-\omega t)] \tag{49}$$

At each typical lattice node j there are two freedoms: v_j and θ_j. Two patch equations are extracted, and converted to dimensionless form on defining $\kappa=k\ell$ and $\Omega=\omega c/\ell$, in which $c=EI/(\rho A\ell^4)$ is a reference phase velocity. (Do not confuse with c_0.) The condition for wave propagation gives the characteristic matrix equation

$$\det\begin{bmatrix}C_{vv} & C_{v\theta}\\ C_{\theta v} & C_{\theta\theta}\end{bmatrix}=C_{vv}C_{\theta\theta}-C_{v\theta}C_{\theta v}=0 \tag{50}$$

where the coefficients are complicated functions not listed there. Solving the equation provides two equations: Ω_a^2 and Ω_o^2, where a and o denote acoustic and optical branch, respectively. These are expanded in powers of κ for matching to the continuum. For the full mass matrix one obtains

$$\Omega_a^2=\kappa^4+C_6\kappa^6+C_8\kappa^8+C_{10}\kappa^{10}+\cdots,\quad \Omega_o^2=D_0+D_2\kappa^2+\cdots \tag{51}$$

Coefficients up to κ^{12} were computed by Mathematica. Relevant ones for parameter selection are

$$C_6=-\Phi/12-\Psi^2$$

$$C_8=[2-15\mu_{R2}-\mu_{T2}+5\Phi(1+\Phi)+60(1+3\Phi)\Psi^2+720\Psi^4]/720$$

$$C_{10}=[-44+35\mu_{T2}-3\mu_{T3}-282\Phi+525\mu_{R2}(1+\Phi)-105\mu_{R3}(1+\Phi)+1{,}575\mu_{R2}\Phi(1+\Phi)-\Phi(3\mu_{T3}-35\mu_{T2}(4+3\Phi)+35\Phi(17+5\Phi(3+\Phi)))+(-2{,}940+12{,}600\mu_{R2}(1+\Phi)+420(2\mu_{T2}(1+\Phi)-5\Phi(7+6\Phi(2+\Phi))))\Psi^2-25{,}200(2+\Phi(7+6\Phi))\Psi^4-302{,}400(1+\Phi)\Psi^6]/[302{,}400(1+\Phi)]$$

$$D_0=25{,}200(1+\Phi)/[7+105\mu_{R2}+3\mu_{T3}+2{,}100\Phi^2\Psi^2]$$

$$D_2=[2{,}100(1+\Phi)(-56-35\mu_{T2}+3\mu_{T3}-63\Phi+3\mu_{T3}\Phi+105\mu_{R3}(1+\Phi)-525\mu_{R2}(1+\Phi)^2-35\mu_{T2}\Phi(2+\Phi))+2{,}100(1+\Phi)(3{,}360\Phi+6{,}300\Phi^2+2{,}100\Phi^3)\Psi^2+52{,}920{,}000\Phi^2(1+\Phi)\Psi^4]/[7+105\mu_{R2}+3\mu_{T3}+2{,}100\Phi^2\Psi^2]^2 \tag{52}$$

For the block-diagonal template (47)

$$\Omega_a^2=\kappa^4+F_6\kappa^6+F_8\kappa^8+F_{10}\kappa^{10}+\cdots,\quad \Omega_o^2=G_0+G_2\kappa^2+\cdots \tag{53}$$

where

$$F_6=-24\nu_2-\Phi,\quad F_8=\frac{2880\nu_2-5\Phi+360\nu_2\Phi-1-5\Phi+5\Phi^2}{720}$$

$$G_0=\frac{6}{\nu_2(1+\Phi)},\quad G_2=\frac{24\nu_2+\Phi-2}{2\nu_2(1+\Phi)} \tag{54}$$

The expansions for the seven-parameter template (48) are considerably more complicated than the previous ones, and are omitted to save space.

J. Aerosp. Eng., 2006, 19(4): 241-258

Table 3. Useful Template Instances for Timoshenko Beam Element

Instance name	Description	Comments
CMM	Consistent mass matrix of Archer. Matches flexural branch up to $O(\kappa^6)$.	A popular choice. Fairly inaccurate, however, as beam gets thicker. Grossly overestimates intermediate frequencies.
FBMS	Flexural-branch matched to $O(\kappa^{10})$ with spectral (Legendre) template (45).	Converges faster than CMM. Performance degrades as beam gets thicker, however, and element becomes inferior to CDLA.
SBM0	Shear branch matched to $O(\kappa^0)$ while flexure fitted to $O(\kappa^{10})$	Custom application: To roughly match shear branch and cutoff frequency as mesh is refined. Danger: Indefinite for certain ranges of Φ and Ψ. Use with caution.
SBM2	Shear branch matched to $O(\kappa^2)$ while flexure fitted to $O(\kappa^8)$	Custom application: To finely match shear' branch and cutoff frequency as mesh is refined. Danger: Indefinite for wide ranges of Φ and Ψ. Use with extreme caution.
DLMM	Diagonally lumped mass matrix with rotational mass picked to match flexural branch to $O(\kappa^6)$.	Obvious choice for explicit dynamics. Accuracy degrades significantly, however, as beam gets thicker. Underestimates frequencies. Becomes singular in the Bernoulli-Euler limit.
CDLA	Average of CMM and DLMM. Matches flexure branch to $O(\kappa^8)$.	Robust all-around choice. Less accurate than FBMS and FBMG for thin beams, but becomes top performer as aspect ratio increases. Easily constructed if CMM and DLMM available in code.
FBMG	Flexural branch matched to $O(\kappa^{10})$ with seven-parameter template (48).	Known to be the globally optimal positive-definite choice for matching flexure in the Bernoulli-Euler limit. Accuracy, however, is only marginally better than FBMS. As in the case of the latter, performance degrades as beam gets thicker.

Template Instances

Seven useful instances of the foregoing templates are identified and described in Table 3. Table 4 lists the template signatures that generate those instances. These tables include two existing mass matrices (CMM and DLMM) re-expressed in the template context, and five new ones. The latter were primarily obtained by matching series such as Eqs. (52) and (53) to the continuum ones [Eqs. (33) and (34)], up to a certain number of terms as described in Table 3.

For the spectral template it is possible to match the flexure branch up to $O(\kappa^{10})$. Trying to match $O(\kappa^{12})$ leads to complex solutions. For the diagonal template the choice is more restrictive. It is only possible to match flexure up to $O(\kappa^6)$, which leads to instance DLMM. Trying to go further gives imaginary solutions. For the seven-parameter template (48) it is again possible to match up to $O(\kappa^{10})$ but no further. The instance that exhibits the least truncation error while retaining positivity is FBMG. This is globally optimal for the Bernoulli-Euler limit $\Phi=\Psi=0$, but the results are only slightly better for the reasons discussed in section entitled "Optimal mass matrices for the Bernoulli-Euler Beam". Matching both flexure and shear branches leads to instances SBM0 and SBM2, which have the disadvantages noted in Table 3.

The exact dispersion curves of these instances are shown in Fig. 12 for $\Phi=48/125$ and $\Psi^2=1/75$, which pertains to a thick beam. On examining Fig. 12(c) it is obvious that trying to match the shear branch is difficult; the fit only works well over a tiny range near $\kappa=0$.

Vibration Analysis Example

The performance of the seven instances of Tables 3 and 4 for vibration analysis is evaluated on a simply supported prismatic beam of length L divided into N_e equal elements. The cross section is rectangular with width b and height h. The material is isotropic with Poisson's ratio $\nu=0$. Three different height-to-span ratios h/L, characterizing a thin, moderately thick and thick beam, respectively, are considered. Results for these configurations are collected in Figs. 13–15, respectively, for the first three

Table 4. Template Signatures for Mass Matrices of Table 3

Instance name	Template form	Template signature							Fit to continuum frequencies	
		μ_{T2}	μ_{T3}	μ_{R2}	μ_{R3}	ν_1	ν_2	μ_0	Ω_f^2 (flexural)	Ω_s^2 (shear)
CMM	(45)	1	1	$4\Psi^2$	$4\Psi^2$				Up to κ^6	None
FBMS	(45)	2	26/3	$4\Psi^2+\Phi/3$	c_1				Up to κ^{10}	None
SMB0	(45)	2	−7/3	$4\Psi^2+\Phi/3$	$20\Phi\Psi^2$				Up to κ^{10}	Up to κ^0
SMB2	(45)	2	−7/3	c_2	$20\Phi\Psi^2$				Up to κ^8	Up to κ^2
DLMM	(47)					0	$\frac{1}{2}\Psi^2$		Up to κ^6	None
CDLA	(48)	1	1	$4\Psi^2$	$4\Psi^2$	0	$\frac{1}{2}\Psi^2$	1/2	Up to κ^8	None
FBMG	(48)	c_3	c_4	c_5	c_6	1/12	$\frac{1}{2}\Psi^2$	c_7	Up to κ^{10}	None

Note: $c_1=(25\Phi^3+120\Psi^2+\Phi^2(45-300\Psi^2)+3\Phi(7-20\Psi^2+1200\Psi^4))/(15(1+\Phi))$; $c_2=(-19+10\Phi^2(90\Psi^2-1)-30\Phi(1-26\Psi^2+120\Psi^4))/(75(1+\Phi)^2)$; $c_3=(9+\sqrt{105})/10$; $c_4=(61\sqrt{105}-483)/18$; $c_5=(\sqrt{105}-1)\Phi/30$; $c_6=(-48\Phi+727\Phi^2+840\Phi^3+22{,}128\Psi^2+19{,}848\Phi\Psi^2-10{,}080\Phi^2\Psi^2-113{,}040\Psi^4+120{,}960\Phi\Psi^4+5\sqrt{105}(48\Phi+87\Phi^2+40\Phi^3)-24(6+21\Phi+20\Phi^2)\Psi^2+720(3+8\Phi)\Psi^4)/(60(21+\sqrt{105})(1+\Phi))$; and $c_7=(3-5\sqrt{5/21})/8$.

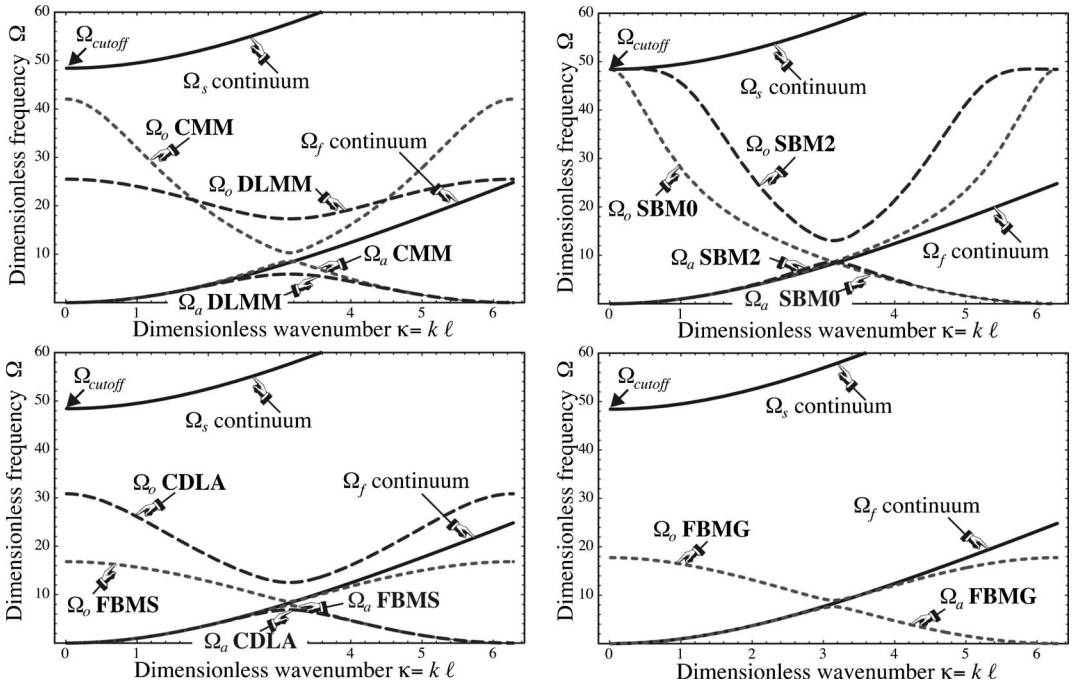

Fig. 12. Dimensionless dispersion curves of Timoshenko mass matrices instances of Tables 3 and 4 for a thick beam with $\Phi_0=48/125=0.384$ and $\Psi_0^2=1/75=0.0133$. (a) Curves for standard consistent and diagonally lumped matrices CMM and DLMM; (b) curves for the flexural-branch-matched FBMS and CDLA; (c) curves for the shear-branch-matched SBM0 and SBM2; and (d) curve for flexure-branch globally optimized FBMG.

vibration frequencies. All calculations are rendered dimensionless using the scaling techniques described previously.

Vibration accuracy is displayed as log-log plots of dimensionless natural frequency error versus N_e. The error is displayed as $d=\log_{10}(|\Omega_{\text{comp}}-\Omega_{\text{exact}}|)$, which gives at a glance the number of correct digits d, versus $\log_2 N_e$ for $N_e=1-32$. Should the error be approximately controlled by a truncation term of the form $\propto\kappa^m$, the log-log plot should be roughly a straight line of slope $\propto m$, since $\kappa=k\ell=kL/N_e$.

The results for the Bernoulli-Euler model, shown in Fig. 13, agree perfectly with the truncation error in the Ω_f^2 branch as listed in Table 4. For example, top performers FBMG and FBMS gain digits twice as fast as CMM, DLMM, and SBM2, as the formers match Ω_f^2 to $O(\kappa^{10})$ whereas the latter do that only to $O(\kappa^6)$. Instances CDLA and SMB0, which agree through $O(\kappa^8)$, come in between. The highly complicated FBMG is only slightly better than the simpler FBMS. Their high accuracy should be noted. For

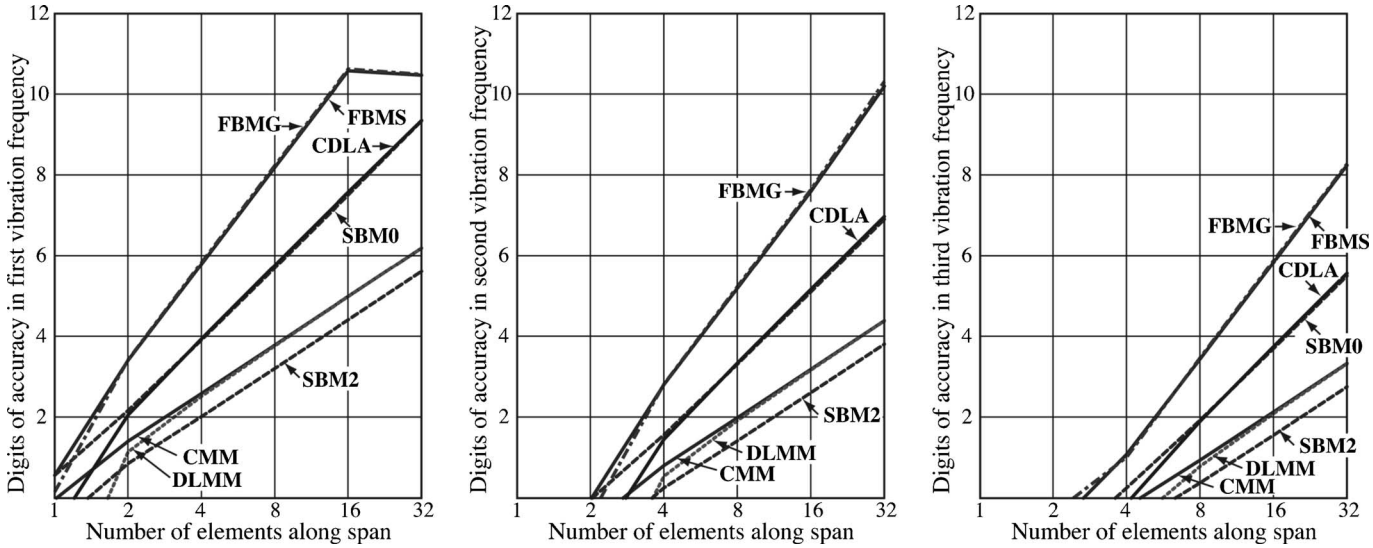

Fig. 13. Accuracy of first three natural vibration frequencies of SS prismatic beam using the mass matrices of Tables 3 and 4. Bernoulli-Euler model with $\Phi_0=\Psi_0=0$. Exact (to 12 places) frequencies $\Omega_1=\pi^2=9.869604401089$, $\Omega_2=4\pi^2=39.478417604357$, and $\Omega_3=9\pi^2=88.826439609804$. Cutoff frequency $+\infty$.

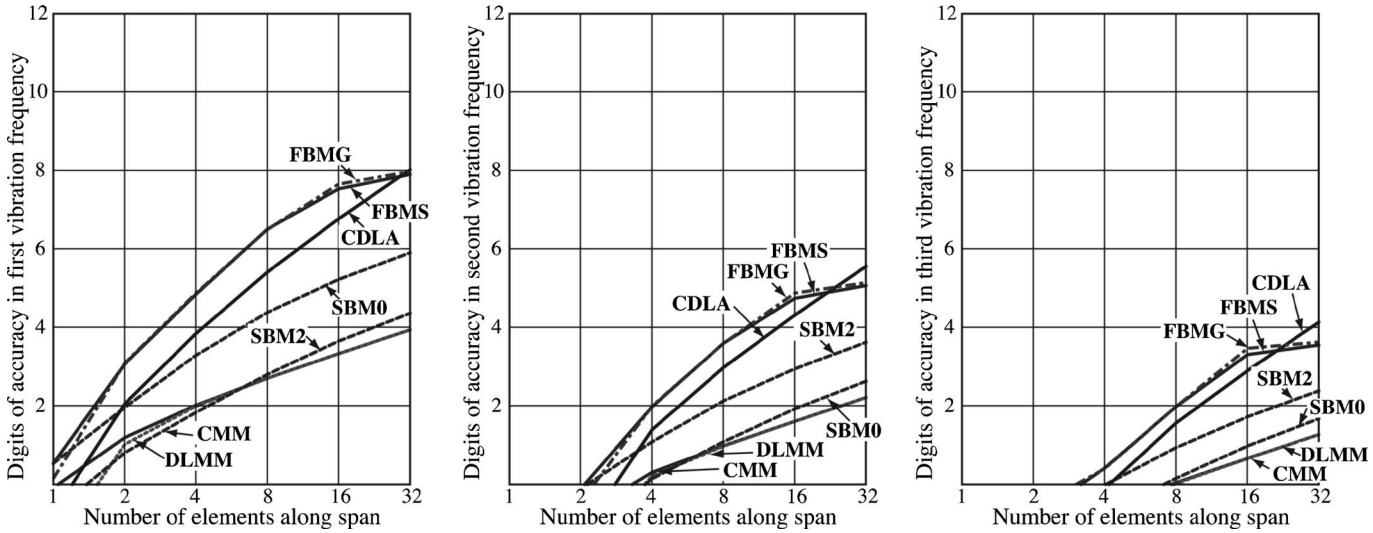

Fig. 14. Accuracy of first three natural vibration frequencies of SS prismatic beam using the mass matrices of Tables 3 and 4. Timoshenko model with $\Phi_0=3/80=0.0375$ and $\Psi_0^2=1/768=0.00130$, pertaining to a rectangular cross section with $h/L=1/8$ and $\nu=0$. Exact (to 12 places) frequencies $\Omega_1=9.662562122511$, $\Omega_2=36.507937703548$, and $\Omega_3=75.894968024537$. Cutoff frequency $\Omega_{\text{cut}}=12/(\Phi_0\Psi_0^2)=495.741868314549$.

example, four FBMS elements give Ω_1 to six figures: 9.86960281… versus $\pi^2=9.86960440\ldots$, whereas CMM gives less than three: 9.87216716…. The "accuracy ceiling" of approximately 11 digits for FBMS and FBMG observable for $N_e>16$ is due to the eigensolver working in double precision ($\approx$ 16 digits). Rerunning with higher (quad) floating point precision, the plots continues marching up as straight lines before leveling at about 25 digits.

On passing to the Timoshenko model, the well ordered Bernoulli-Euler world of Fig. 13 unravels. The culprits are Φ and Ψ. These figure prominently in the branch series and grow without bound as N_e increases, as discussed in section entitled "Beam Element." Fig. 14 collects results for a moderately thick beam with $h/L=1/8$, which corresponds to $\Phi_0=3/80$ and $\Psi_0^2=1/768$. The Bernoulli-Euler top performers, FBMS and FBMG, gradually slow down and are caught by CDLA by $N_e=32$. All other instances trail, with the standard ones: CMM and DLMM, becoming the worst performers. Note that for $N_e=32$, CMM and DLMM provide only 1 digit of accuracy in Ω_3 although there are $32/1.5\approx 21$ elements per wavelength

Fig. 15 collects results for a thick beam with $h/L=2/5$, corresponding to $\Phi_0=24/625$ and $\Psi_0^2=1/75$. The foregoing trends are exacerbated, with FBMS and FBMG running out of steam by $N_e=4$ and CDLA emerging as best for $N_e\geqslant 8$. Again DLMM and CMM trail badly.

The reason for the performance degradation of FBMS and FBMG as the Timoshenko beam gets thicker is not clear as of this writing. Eigensolver accuracy is not responsible since rerunning the cases of Figs. 14 and 15 in quad precision did not change the plots. A numerical study of the Ω_f^2 truncation error shows that FBMS and FBMG fit the continuum branch better than CDLA even for very thick beams. Possible contamination of vibration mode shapes with the shear branch was not investigated.

Optimal Mass Matrices for the Bernoulli-Euler Beam

It was observed in the numerical vibration experiments that for the Bernoulli-Euler model, the top performers (in that limit) FBMS and FBMG furnished near identical results despite coming from templates with four and seven parameters, respectively. The near coalescence can be explained as follows. Specializing the FBMS instance to $\Phi=\Psi=0$ yields

$$\mathbf{M}_S^e=\frac{\rho A\ell}{12{,}600}\begin{bmatrix}4818 & 729\ell & 1482 & -321\ell\\ & 172\ell^2 & 321\ell & -73\ell^2\\ & & 4818 & -729\ell\\ \text{symm} & & & 172\ell^2\end{bmatrix}=\rho A\ell\begin{bmatrix}0.382381 & 0.057857\ell & 0.117619 & -0.025476\ell\\ & 0.013651\ell^2 & 0.025476\ell & -0.005794\ell^2\\ & & 0.382381 & -0.057857\ell\\ \text{symm} & & & 0.013651\ell^2\end{bmatrix} \quad (55)$$

The flexural branch of the continuum Bernoulli-Euler model is exactly $\Omega_f^2=\kappa^4$. A FEM patch with mass (55) matches it up to $O(\kappa^{10})$, and has a truncation error $C_{12}\kappa^{12}$, with $C_{12}=-41/18{,}144{,}000\approx -2.25\times 10^{-6}$.

Specializing the FBMG instance the same way yields

$$\mathbf{M}_G^e=\frac{\rho A\ell}{30{,}240}\begin{bmatrix}a_{11} & 1788\ell & a_{13} & -732\ell\\ & a_{22}\ell^2 & 732\ell & a_{24}\ell^2\\ & & a_{33} & 1788\ell\\ \text{symm} & & & a_{44}\ell^2\end{bmatrix}=\rho A\ell\begin{bmatrix}0.389589 & 0.059127\ell & 0.110410 & -0.024206\ell\\ & 0.012340\ell^2 & 0.024206\ell & -0.005548\ell^2\\ & & 0.389589 & -0.059127\ell\\ & & & 0.012340\ell^2\end{bmatrix} \quad (56)$$

J. Aerosp. Eng., 2006, 19(4): 241-258

in which $a_{11}=a_{33}=12{,}396-60\sqrt{105}$, $a_{13}=2{,}724+60\sqrt{105}$, $a_{22}=a_{44}=117+25\sqrt{105}$, and $a_{24}=-219+5\sqrt{105}$. The flexure branch truncation error is again $C_{12}\kappa^{12}$ with $C_{12}=(25\sqrt{105}-441)/91{,}445{,}760\approx-2.06\times10^{-6}$, which is only about 10% smaller. Consequently the practical difference between the optimal spectral matrix and the globally optimal one is not significant. Because both truncation errors are of the same sign, a C_{12}-canceling linear combination that keeps mass positivity is not feasible.

Historical Notes and Comments

As narrated in Felippa (2001c), the first appearance of a mass matrix in a journal article occurs in two early-1930s papers by Duncan and Collar (1934, 1935). Therein it is called "inertia matrix" and denoted by $[m]$. The original example of Duncan and Collar (1934, p. 869) displays the 3×3 diagonal mass of a triple pendulum. In the book of Frazer et al. (1938) the notation changes to A.

DLMM dominate pre-1963 work. Computational simplicity was not the only reason. Direct lumping gives an obvious way to account for *nonstructural masses* in simple discrete models of the spring-dashpot-pointmass variety. For example, in a multistory building "stick model," where each floor is treated as one DOF in lateral sway under earthquake or wind action, it is natural to take the entire mass of the floor (including furniture, isolation, etc.) and assign it to that freedom. Nondiagonal masses appeared occasionally in aircraft matrix analysis—e.g., wing oscillations in Sec. 10.11 of Frazer et al. (1938)—as a result of measurements. As such they necessarily accounted for nonstructural masses due to fuel, avionics, etc.

The formulation of the CMM by Archer (1963, 1965) was a major advance. The underlying theory is old; in fact it follows directly from the Lagrange dynamic equations, which is a two-century-old proven technique to produce generalized masses. If T is the kinetic energy of a discrete system and $\dot{u}_i(x_i)$ the velocity field defined by the nodal velocities collected in $\dot{\mathbf{u}}$, the master (system level) $\mathbf{M}$ can be defined as the Hessian of T with respect to nodal velocities

$$T=\frac{1}{2}\int_\Omega \rho\dot{u}_i\dot{u}_i d\Omega,\quad u_i=u_i(\dot{\mathbf{u}}),\quad \mathbf{M}=\frac{\partial^2 T}{\partial\dot{\mathbf{u}}\,\partial\dot{\mathbf{u}}} \tag{57}$$

This matrix is constant if T is quadratic in $\dot{\mathbf{u}}$. Some implementation decisions had to be worked out before use in FEM: localization by applying (57) element-by-element and the master $\mathbf{M}$ assembled, and interpolation of the velocity field by the same shape functions as displacements. These in turn had to wait until three tools became well established by the early 1960s: (1) the direct stiffness method of Turner; (2) the concept of shape functions; and (3) the FEM connection to Rayleigh-Ritz. The critical ingredient (3) was established in the thesis of Melosh (1962) under Harold Martin, and the subsequent journal article by Melosh (1963). The link to dynamics was closed with Archer's contributions, and CMM became a staple of FEM. But only a loose staple. Problems persisted:

1. Nonstructural masses are not naturally handled by CMM. In systems such as ships or aircraft, the structural mass may be only a small fraction of the total.
2. It is inefficient in some solution processes, notably explicit dynamics.
3. It may not give the best results compared to other alternatives. For example, if the stiffness matrix results from a conforming displacement interpolation, pairing it with the CMM becomes conventional Rayleigh-Ritz, and thus provides upper bounds on natural frequencies. This is not necessarily a good thing. If the response is strongly influenced by intermediate and high frequencies, as in wave propagation dynamics, the CMM may give poor results. The weak performance of the CMM displayed in Figs. 14 and 15 for the Timoshenko beam is not atypical.
4. For elements derived outside the assumed-displacement framework, velocity shape functions may be unknown or altogether missing.

Problem (1) can be addressed by constructing "rigid mass el-

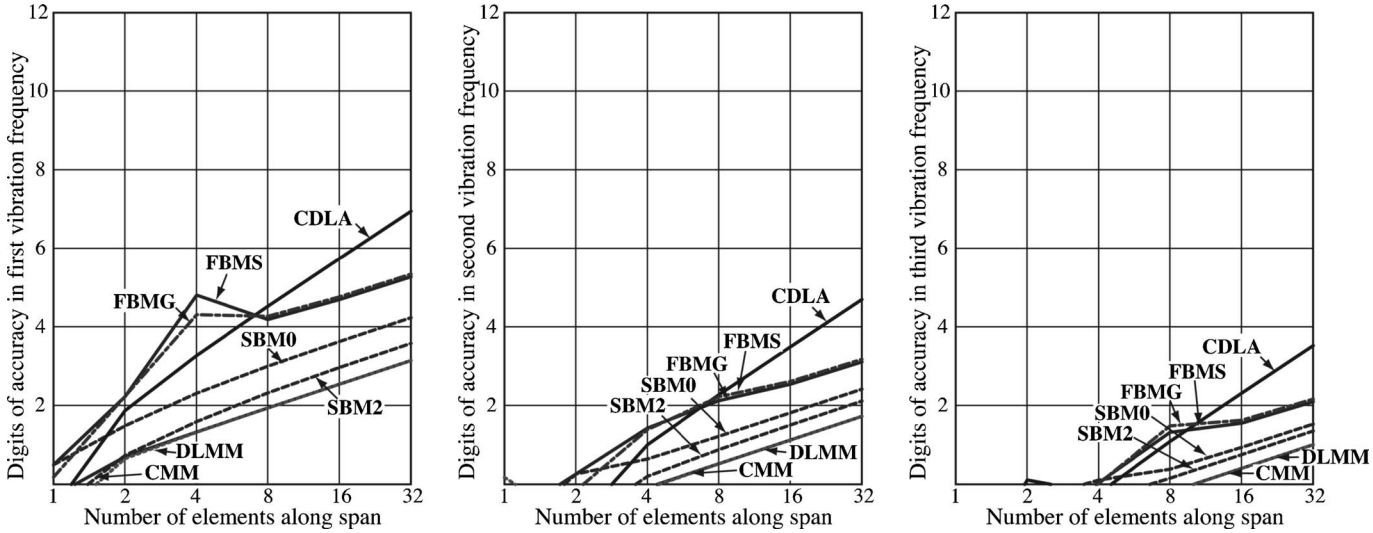

Fig. 15. Accuracy of first three natural vibration frequencies of SS prismatic beam using the mass matrices of Tables 3 and 4. Timoshenko model with $\Phi_0=24/625=0.384$ and $\Psi_0^2=1/75=0.0133$, pertaining to a rectangular cross section with $h/L=2/5$ and $\nu=0$. Exact (to 12 places) frequencies $\Omega_1=8.287891683498$, $\Omega_2=24.837128591729$, and $\Omega_3=43.182948411234$. Cutoff frequency $\Omega_{\text{cut}}=12/(\Phi_0\Psi_0^2)=48.412291827593$.

ements" accounting for inertia (and possibly gravity or centrifugal forces) but no stiffness. Nodes of such elements must be linked to structural (elastic) nodes by multifreedom constraints that enforce kinematic constraints. This is more of an implementation issue than a research topic, although numerical difficulties typical of rigid body dynamics may arise.

Problems 2–4 can be attacked by parametrization. MacNeal (1970) was the first to observe that averaging the DLMM and CMM of the two-node bar element gave better results than either alone. This is covered in the book of MacNeal (1994). The idea was further studied by Belytschko and Mullen (1978) using Fourier analysis. Earlier, Krieg and Key (1972) had already emphasized that in transient analysis the introduction of a time discretization operator brings new compensation phenomena, and consequently the time integrator and the mass matrix should not be be chosen separately.

The template approach addresses problems 2–4 by allowing and encouraging full customization of the mass matrix to the problem and solution method at hand. The method was originally developed to construct high-performance stiffness matrices; a historical account and pertinent references are provided in a recent tutorial by Felippa (2004). For stiffness-mass pairs it was used by Felippa (2001a, b) for a Bernoulli-Euler plane beam treated by Fourier analysis. One idea developed in those papers but not pursued here was to include the stiffness matrix template in the customization process. This provides more flexibility but has a negative side: highly optimized stiffness-mass pairs become sensitive to mesh distortion.

The symbolic derivation scheme used for the EOM (30) was first used in the thesis of Flaggs (1988); see also the article by Park and Flaggs (1984).

Making $\mathbf{K}$ and $\mathbf{M}$ frequency dependent was proposed by Przemieniecki (1968), who expanded both $\mathbf{K}^e$ and $\mathbf{M}^e$ as Taylor series in ω^2. The idea was applied to eigenfrequency analysis of bars and beams, but not pursued further. The approach can be generalized to the template context by making free parameters frequency dependent, as illustrated in the two-node bar example of the section entitled "Best μ by Fourier Analysis." This may be of interest for problems dominated by a single driving frequency, as in some electronic and optical components. For more general use keeping the parameters frequency independent, as done in the other two examples, appears to be more practical.

Two powerful customization techniques used regularly for templates are Fourier methods and modified differential equations. Fourier methods are limited to separable systems but can be straightforward to apply, requiring only undergraduate mathematics. [As tutorials for applied Fourier methods the textbooks by Hamming (1973, 1998) are recommended.] Modified differential equation methods, first published in correct form in Warming and Hyett (1974) are less restrictive but more demanding on two fronts: mathematical ability and support of a CAS. Processing power limitations presently restrict these methods to 2D elements and regular meshes. The selection of template optimization criteria is not yet on firm ground. For example: is conservation of angular momentum useful in mass templates? The answer seems to depend on the element complexity.

Results for regular lattices of structural elements have direct counterparts in a very different area: Molecular physics. More precisely, the wave mechanics of crystalline solids created in the XX Century by particle mechanicians, e.g., Born and Huang (1954) and Ziman (1967). In crystal models, lattice nodes are occupied by molecules interacting with adjacent ones. Thus the "element dimension" ℓ acquires a physical meaning of molecular gap. In those applications masses are always *lumped* at molecule locations, and atoms vibrate as harmonic oscillators in the potential well of the force fields of their neighbors. Dispersion curves govern energy transmission. In a linear atomic chain, the wavenumber range $\kappa \in [-\pi, \pi]$ is called the first Brillouin zone, a topic covered by Brillouin (1946) and Jones (1960). Such a connection may be of interest as FEM and related discretization methods are extended into nano-mechanics.

Acknowledgments

The pioneering contributions of Professor Noor to two of the tools heavily used in this paper: continuification of dynamic lattices as surveyed in Noor (1988) and the use of CAS in computational mechanics as discussed in Noor and Andersen (1979), are gratefully acknowledged. Preparation of this paper has been supported by the National Science Foundation under Grant No. CMS–0219422.

References

Archer, J. S. (1963). "Consistent mass matrix for distributed mass systems." *J. Struct. Div.*, 89, 161–178.

Archer, J. S. (1965). "Consistent mass matrix formulation for structural analysis using finite element techniques." *AIAA J.*, 3, 1910–1918.

Belytschko, T., and Mullen, R. (1978). "On dispersive properties of finite element solutions." *Modern problems in elastic wave propagation*, J. Miklowitz and J. D. Achenbach, eds., Wiley, New York, 67–82.

Born, M., and Huang, K. (1954). *Dynamical theory of crystal lattices*, Oxford, London.

Brillouin, L. (1946). *Wave propagation in periodic structures*, Dover, New York.

Duncan, W. J., and Collar, A. R. (1934). "A method for the solution of oscillations problems by matrices." *Philos. Mag.*, Series 7, 17, 865–885.

Duncan, W. J., and Collar, A. R. (1935). "Matrices applied to the motions of damped systems." *Philos. Mag.*, Series 7, 19, 197–214.

Felippa, C. A. (2001a). "Customizing high performance elements by Fourier methods." *Trends in computational mechanics*, W. A. Wall et al., eds., CIMNE, Barcelona, Spain, 283–296.

Felippa, C. A. (2001b). "Customizing the mass and geometric stiffness of plane thin beam elements by Fourier methods." *Eng. Comput.*, 18, 286–303.

Felippa, C. A. (2001c). "A historical outline of matrix structural analysis: a play in three acts." *Comput. Struct.*, 79, 1313–1324.

Felippa, C. A. (2004). "A template tutorial." *Computational mechanics: Theory and practice*, Chap. 3, K. M. Mathisen, T. Kvamsdal, and K. M. Okstad, eds., CIMNE, Barcelona, 29–68.

Flaggs, D. L. (1988). "Symbolic analysis of the finite element method in structural mechanics." Ph.D. dissertation, Dept. of Aeronautics and Astronautics, Stanford University.

Frazer, R. A., Duncan, W. J., and Collar, A. R. (1938). *Elementary matrices, and some applications to dynamics and differential equations*, Cambridge University Press, Cambridge, U.K.

Hamming, R. W. (1973). *Numerical methods for scientists and engineers*, 2nd Ed., Dover, New York.

Hamming, R. W. (1998). *Digital filters*, 3rd Ed., Dover, New York.

Jones, H. (1960). *The theory of Brillouin zones and electronic states in crystals*, North-Holland, Amsterdam, The Netherlands.

Krieg, R. D., and Key, S. W. (1972). "Transient shell analysis by numerical time integration." *Advances in computational methods for structural mechanics and design*, J. T. Oden, R. W. Clough, and Y. Yamamoto, eds., UAH, Huntsville, Ala., 237–258.

MacNeal, R. H., ed. (1970). "The NASTRAN theoretical manual." *NASA Rep. No. SP-221*.

MacNeal, R. H. (1994). *Finite elements: Their design and performance*, Marcel Dekker, New York.

Melosh, R. J. (1962). "Development of the stiffness method to define bounds on the elastic behavior of structures." Ph.D. dissertation, Dept. of Engineering Mechanics, Univ. of Washington, Seattle.

Melosh, R. J. (1963). "Bases for the derivation of matrices for the direct stiffness method." *AIAA J.*, 1, 1631–1637.

Noor, A. K. (1988). "Continuum modeling for repetitive lattice structures." *Appl. Mech. Rev.*, 41 (7), 285–296.

Noor, A. K., and Andersen, C. M. (1979). "Computerized symbolic manipulation in structural mechanics—Progress and potential." *Comput. Struct.*, 10, 95–118.

Park, K. C., and Flaggs, D. L. (1984). "An operational procedure for the symbolic analysis of the finite element method." *Comput. Methods Appl. Mech. Eng.*, 46, 65–81.

Przemieniecki, J. S. (1968). *Theory of matrix structural analysis*, McGraw-Hill, New York.

Warming, R. F., and Hyett, B. J. (1974). "The modified equation approach to the stability and accuracy analysis of finite difference methods." *J. Comput. Phys.*, 14, 159–179.

Ziman, J. M. (1967). *Principles of the theory of solids*, North-Holland, Amsterdam, The Netherlands.